Please note that this electronic version does not contain the full thesis. Some figures and included papers are missing.

Some Control Applications in Electric Power Systems

Magnus Akke

Doctoral Dissertation
April 11, 1997

Department of Industrial Electrical Engineering and Automation
Lund University, Sweden

Chapter 1

Introduction

This thesis is a collection of control papers. It consists of two parts. The first one aims to bind the themes together. The second one is a set of published, or submitted, papers. When I considered a suitable title, three words came to my mind: *potpourri*, *medley* and *blend*. The American Heritage Dictionary provides the following explanations of these words.

Potpourri is:

- a combination of incongruous things;
- a miscellaneous anthology or collection.

Medley is:

- an often jumbled assortment; a mixture;
- a music arrangement made from a series of melodies, often from various sources.

Blend is:

- to combine (varieties or grades) to obtain a mixture of a particular character, quality, or consistency;
- to form a uniform mixture; intermingle;
- to create a harmonious effect or result.

Obviously there is not any plain concise word for a mixture of control papers applied to power systems, even though some ideas sparkled up. What about: “Control Medley in the Muddy Waters of Power Systems”, or, “Control Potpourri Orchestrated in Power Systems” or even the more cryptic “A Power Connoisseurs Blend of Control Applications”? These titles might attract more curiosity, but could be slightly misleading from a scientific point of view. With some guidance from my supervisors the final choice of title was the somewhat less extrovert “Some Control Applications in Electric Power Systems”. I hope that the title will reflect the content of the thesis and attract the appropriate readers.

1.1 Background

This thesis consist of four papers. At a first glance it might be unclear what the common factors of the papers are. The purpose can be seen from two different perspectives. The thesis can be regarded with a down-to-earth view, interpreting just the meaning of the title. It just shows some examples of control applications in power systems. The punch-line is that control can be useful in power systems. The second view-point takes a broader perspective and says that it is more than just some examples. The thesis shows that control theory and, even more, control research and post-grad education are relevant for industry.

Each paper is motivated by a practical problem. Also, to the best of my knowledge, the work presented in the papers have given my employer economic benefit. The most obvious example is presented in the papers [7, 8]. This work started because a 300 million US-dollar project was halted by the German authority who is responsible for sea safety. They would not grant permission for the Baltic Cable HVDC-link unless the project could show the DC-cable's effect on sea traffic. Ships with auto-pilots that used a magnetic compass were of special concern. A study was made that included theory, simulations and field tests. The results were presented to the German sea authorities. Because of the technical quality of the study, permission was granted and the future of the Baltic Cable HVDC link was secured. The project could continue and the link was later commissioned in 1994.

This chapter presents some general ideas on how to succeed with control applications. The outline of the thesis is presented at the end of the chapter.

1.2 Application of Control Theory

Methodology

Methodology is of utmost importance to successfully apply control. This can not be over-emphasized. Theory, simulations, field tests and evaluation are the key ingredients in a basic control application recipe. Often the procedure has to be iterated. If the field tests show unmodeled dynamics, the model needs refinements. If the field results can not be understood, we have to question if the appropriate theory has been used.

When I started at Sydkraft, I was fortunate to have Tech. Lic. Sture Lindahl as my tutor. He pursued the method of alternating between theory and field measurements. Even though not the easiest, it is the best way to understand and solve control problems. Some examples of work done under his guidance are presented in [1-12].

In recent years there has been a tendency in control that research is categorized as either theoretical or experimental. Sometimes, the theorists get accused of losing contact with reality. If the theorist can not apply his own control theory, how can he expect somebody else to do it? The industry needs engineers that can digest theoretical work, pick out the relevant parts and apply them.

The control society is very active in publishing papers. It is a full time effort to keep pace with the development of new theory. Still, many industrial control problems, that are relatively simple, remain unsolved. The purpose of this thesis is to show, by example, that control theory is a very useful tool for practical problems. By doing so, I hope to reduce the gap between theory and application. At best, this will stimulate the theorist to apply his knowledge and the practical engineer to use a bit more theory.

The Swedish Heritage

At Swedish universities, control theory is taught as a general subject. Only one department at each university is responsible for control. At foreign universities it is common to have a control group within each major department, so, electrical engineering has one control group, chemical engineering has another, and so forth. It has become a Swedish tradition to emphasize that control theory provides general tools that can be applied to problems in many different fields. Some successful examples are: step size control in ordinary differential equation (ODE) solvers; control of resonant servo systems; object oriented modeling of chemical processes; adaptive control of ship steering; analysis of power system stability.

Professor Karl Johan Åström has been the *primus motor* for the "Swedish Control Tradition". Back in the good old days, he initiated several full scale experiments such as identification of boiler dynamics [13] in the late 1960s, and adaptive control of supertankers in the 1970s [14]. By using advanced theory, he gave industry improved solutions to practical problems. The unique combination of scientist/salesman gave control theory industrial credibility. The key idea was to cross-fertilize novel control methods with industrial applications. Adaptive control was one baby born and bred by this idea. Students were attracted to automatic control, which both stimulated the intellect and also provided an entrance ticket to high tech industry. Some of Karl Johan's disciples have followed his trajectory, some have diverged.

After two decades as Åström's right hand, Professor Gustaf Olsson got his own professor chair. His—and Professor Alakula's—department has a profile that offers both theoretical resources and laboratory facilities to perform experiments. This suited my project.

Swedish engineers graduate with knowledge of general control theory. The idea has been that industry should provide the process knowledge needed for each specific application. This thesis shows how this has been done for electric power systems.

Control in Power Systems

In this thesis the controlled process is the electric power system. The North American power system is the largest and most complex machine ever devised by mankind [15]. The smaller Nordel system—consisting of parts of Denmark together with all of Finland, Norway and Sweden —possesses many problems that are great challenges for engineers and scientists. Even though power systems are mature systems, there are still many unexplored areas and unsolved problems. The introduction of microprocessors in power systems has been a revitalizing vitamin injection. It has stimulated the use of novel concepts from control theory, identification and signal processing.

This thesis is devoted to the application of control theory in power systems. All problems presented are existing practical problems. Even with practical problems, though, the appropriate theory is needed. Theory might include discrete and continuous-time control as well as signal processing. The main message is that theory and process knowledge are equally important for control applications in power systems. The thesis aims at a balance between these two objectives.

1.3 Thesis Outline

Each chapter starts with an introduction. References are given at the end of each chapter. Figures are numbered within each chapter. Only the running number is used to refer to a figure within the same chapter. Figures in other chapters are referred to by chapter and figure number, e.g., Figure 2.1 is the first figure in Chapter 2. The same principle is used for references. For example, reference [3.1] is the first reference given in Chapter 3.

Chapter 2 presents a study performed to investigate how a ship steering auto-pilot using a magnetic compass was influenced by the magnetic field from a DC cable. This chapter is an introduction to the paper in Appendix A.

Chapter 3 is devoted to frequency estimation. The frequency estimation problem has been studied both as a general signal processing problem and as an application problem in power systems. In power systems, frequency estimation is important in many relaying applications. The chapter starts with some motivating examples of frequency estimation where the

definition from signal processing has been used. An extensive literature search has been done. Signal processing literature as well as frequency estimation in power systems have been reviewed. Due to space limitations the complete result is not reproduced in this thesis and instead the reader is referred to a separate report. The literature search resulted in a paper that is presented in Appendix B.

Chapter 4 presents results in computer relaying applicable to transmission line protection. Computer relaying is a typical power system application where both control theory and signal processing can be used. Two papers have been produced and are given in Appendix C and D. The papers present improvements in the Differential Equation Algorithm (DEA) for transmission line relaying. It is interesting to find that many problems that arise in computer relaying can be formulated as general signal processing and identification problems. Computer relaying is an interesting application area for signal processing and identification research. Statistical calculations are presented at the end of the chapter. The calculations use an equality that is proved in Appendix E.

Chapter 5 presents field tests performed at the Hemsjö hydro power station, located in southern Sweden. The chapter is a little longer and more self contained than the other chapters, since the results have not yet been published internationally. The purpose of the field tests was to investigate if load switching could be used to improve power system damping.

1.4 References

[1] Akke, M., "Power System Stabilizers in Multimachine System," Licentiate thesis CODEN:LUTFD2/TFRT-3201, Department of Automatic Control, Lund Institute of Technology, Lund, Sweden, 1989.

[2] Akke, M. and Wittenmark, B., "New Analysis and Tuning of Stabilizers in Multimachine Power Systems," *IFAC symposium on Power Systems and Power Plant Control*, Seoul, Korea, August 1989.

[3] Eliasson, B. and Akke, M., "Comparision of Two New Design Methods for Stabilizers in Large Power Systems," *European Control Conference*, Grenoble, France, July 1991.

[4] Akke, M. et al., "On Site Measurements of Generators to Derive Models for Dynamic Simulation Analysis," *9th CEPSI Conference*, Hong Kong, November 1992.

[5] Akke, M. and Karlsson, D., "A Long Term Dynamic Load Model Based on Field Measurements," *IEEE seminar on Electrotechnology*, Bangkok, Thailand, December 1992.

[6a] Akke, M., Axelsson, U., Eriksson, A. and Henning, G., "Development Work Concerning Testing Procedures of Mass Impregnated HVDC Cables," synopsis submitted to *CIGRE Swedish National Committee*, March 15, 1993.

[6b] Eriksson, A., Henning, G., Ekenstierna, B., Axelsson, U. and Akke, M., "Development Work Concerning Testing Procedures of Mass Impregnated HVDC cables," paper 21-206, presented at the *CIGRE Conference*, Paris, France, 28 Aug.-3 Sept., 1994.

[7] Akke, M. and Lampe, K. H., "Interaction of DC Cables and Ship Steering Autopilots," Proceedings of the *33rd IEEE Conference on Decision and Control*, Vol. 4, Lake Buena Vista, Florida, USA, 14-16 December, 1994, pp. 4086-4091.

[8] Akke, M. and Lampe, K. H., "Non-linear Interaction of DC Cables and Magnetically Controlled Ship Steering Autopilots," *IEEE Transactions on Control Systems Technology*, Vol. 3, No. 4, December 1995, pp. 365-376.

[9] Akke, M. et al., "An Object-Oriented Transformer Model in Omola," Proceedings of the *13th World Congress of IFAC*, Volume O, paper 7d-08 5, San Francisco, USA, June 30–July 5, 1996, pp. 259-264.

[10] Akke, M., "Frequency Estimation by Demodulation of Two Complex Signals," paper 96 SM 379-8 PWRD, *IEEE Summer Meeting*, Denver, USA, August 1996.

[11] Akke, M. and Thorp, J. S., "Improved Estimates from the Differential Equation Algorithm by Median Post-Filtering," accepted to the *IEE Conference on Developments in Power System Protection*, University of Nottingham, UK, March 25-27, 1997.

[12] Akke, M. and Thorp, J. S., "Some Improvement in the Three-Phase Differential Equation Algorithm for Fast Transmission Line Protection," submitted to the *IEEE Power Engineering Society* for review, January 1997.

[13] Eklund, K., "Linear Drum Boiler-Turbine Models," Report 7117, Ph.D. thesis, Department of Automatic Control, Lund Institute of Technology, Lund, Sweden, November 1971.

[14] Kȁllstrom, C. G., "Identification and Adaptive Control Applied to Ship Steering," Ph.D. thesis, CODEN: LUTFD2/(TFRT-1018)/1-192/(1979), Department of Automatic Control, Lund Institute of Technology, Lund, Sweden, 1979.

[15] Kundur, P., *Power System Stability and Control*, McGraw-Hill, Inc., New York, USA, 1994.

Chapter 2

Interaction of DC Cables and Ship Steering Autopilots

This chapter presents interaction of submerged DC and magnetically controlled ship steering autopilots. The paper in Appendix A presents the author's contribution.

2.1 Background

Uno Lamm at ASEA, Sweden was a pioneer in the development of HVDC technology. The first commercial HVDC link in the world was taken into service in 1954 and connected Gotland with mainland Sweden [3]. The introduction of thyristor valves made HVDC an attractive alternative for some power applications. The paper in Appendix A lists suitable references on HVDC technology. One application where HVDC is especially useful is for long, typically over 30 km, connections between areas separated by water. Because of the water, a cable is needed. A long AC cable would give too large charging currents, which is one of the reasons for using an HVDC.

2.2 The Baltic Cable HVDC Project

The power utilities Sydkraft AB, Swedish State Power Board (Vattenfall) and PreussenElektra AG, together started the Baltic Cable project. The project aim was to build a 600 MW HVDC connection between Sweden and Germany. A preliminary study was made where different cable routes were investigated. One important question was whether to build a monopolar link with one cable and sea return, or to build a bipolar link with two cables. Sydkraft's expert Sture Lindahl scrutinized the problem. The result showed that a monopolar cable was by far the most economical alternative. Without going into details, it is rather obvious that one thick cable is more cost effective than two thin ones. On the other hand, a monopolar link required some technical development.

One problem was that the progress of HVDC cables had not been as favorable as for HVDC converters. So far the most powerful HVDC cable

was the Fennoskan cable with a rated capacity of 500 MW. In contrast, the Pacific NW-SW link using overhead lines had been commissioned already in 1970 and is a bipole link with 1440 MW converters. To be able to choose the monopolar alternative it was necessary to improve the existing HVDC cables. To serve this purpose the Baltic Cable project started an internal development project without any involvement of cable manufacturers. The result of this work has been reported in [1.6].

A bipolar link uses two cables with current in opposite directions. If the two cables are laid close, the magnetic fields will cancel out. For a monopolar cable there is no cancellation effect. The magnetic field can be large and might influence magnetic compasses. This effect will be pronounced for high currents and shallow water. I believe that Dr. Brilka, a colleague and friend from the German power utility PreussenElektra, was the first project member to raise the question. At the same time, the German sea authorities (WSD=Wasser und Schiffahrt Direction) realized that there could be some magnetic effects from the cable. Then everything happened very quickly.

The German sea authorities declared that Baltic Cable had to clarify the magnetic effects before they could approve the project. The manager got the message: no permission—no Baltic Cable. Something had to be done. A task force was appointed. The German project leader Karl-Heinze Lampe and myself became responsible for the investigation. The prime task was to get the permission to build the HVDC link. We made a full scale investigation that included literature survey, modeling, simulation, field tests and non-linear analysis of the magnetic effect from the HVDC cable. The field tests were performed at the existing Kontiskan HVDC connection between Sweden and Denmark. This link has current amplitude, water depth, and cable direction that were similar to the plans for the Baltic Cable HVDC link. We were especially concerned about interaction with magnetically controlled ship-steering autopilots. As always, we had a lot of help from Tech. Lic. Sture Lindahl. A company, specializing in measurements at sea, was engaged to handle and supply all instrumentation at the field test. It took three days to do all the field tests in 1992. The representatives from WSD were on board the ship for one of the days. Figure 1 shows the ship used at the field tests.

Figure 1. The ship used in the field tests.

The test ship used was of grand bank type, length of 17 m, glass fiber hull, twin engines, twin rudders and with maximal speed of 9 knots. During the tests the ship was equipped with autopilot with interface to magnetic compass, navigation with differential global positioning system (DGPS),

gyro, echo sounder, and digital rudder angle indicator. A personal computer with additional hardware and software was used for data acquisition. The following signals were stored; gyro heading, rudder position, magnetic compass heading, ship positions and time. The ship position was also presented in real time on a navigation screen on board the test ship.

After the test, at a meeting in Kiel, the German sea authorities granted permission for the HVDC link. They motivated their decision with the statement that we had presented an "honest technical investigation with relevant information". When the effects from the DC cable are known, appropriate action can be taken to minimize sea hazards: for example, new sea charts will be printed. The new charts will have warning texts with guidance on how to cross the cable.

The work was first published as a short conference paper at an IEEE-conference [1.7]. The conference paper did not get automatically submitted to a journal. A part was added and the paper was submitted to the IEEE-journal "Control System Technology", where it was later published, see Appendix A.

2.3 Other Recent Publications

Masters thesis

Two students have made a Masters thesis project about interaction between DC cables and ship steering autopilots in 1995. Their task was to make a scaled model that could be used for more experimental tests. A radio controlled boat with a length of 40 cm was used. The experiment was carried out in a swimming pool. The HVDC link was substituted by a car battery and a regular 1.5 mm^2 installation wire. The students managed to reproduce the capture phenomena in the experiments. The master project has been reported in [1].

IEE-paper

After the publication of our paper, a related paper has been presented at an IEE conference [2]. It is not obvious to me whether there is any original contribution in the paper. The paper is more of a summary of internal reports. The section on cable design contains a useful idea about irregularities in the cable route. Unfortunately the authors have missed both our papers and all the references given there.

2.4 References

[1] Fransson, A. and Nilsson, S., “An Experimental Platform for DC Cable Interaction with Ship Steering”, (in Swedish), Master thesis TEIE-5106, Department of Industrial Electrical Engineering and Automation, Lund Institute of Technology, Lund, Sweden, December 1995.

[2] Smith, P. M., Whitlock, J. W. and Balkwill, A. P., “The Effects of HVDC Submarine Cables on Shipping with Magnetic Autopilots,” *IEE Conference on AC and DC Power Transmission*, IEE Conference publication No. 423, 29 April–3 May 1996, pp. 76-80.

[3] Kimbark, E. W., *Direct Current Transmission* , Volume I, John Wiley & Sons, New York, USA, 1971.

Chapter 3

Frequency Estimation

Frequency estimation is the theme of this chapter. The first section gives an introduction to frequency estimation. Section 3.2 contains definitions of instantaneous frequency, instantaneous amplitude and instantaneous phase. Section 3.3 presents some examples that illustrate the use of the definition. Frequency estimation in power systems is discussed in Section 3.4. The author's contribution to frequency estimation is given in Appendix B.

3.1 Introduction

Frequency estimation is applied in a large number of areas. A literature survey [1] shows a large number of references in this area. They can be categorized as signal processing papers, or papers about frequency estimation in power systems, which is our main concern. Due to space constraints the literature survey is presented as a separate report.

A frequency algorithm is a crucial element in many power system applications. It is typically used in equipment for:

- protection against loss of synchronism [14];
- under-frequency and over-frequency relaying (generator protection);
- under-frequency load shedding;
- power system stabilization [13];
- input to other algorithms, for example adaptation of filters for harmonics;
- speed measurement of turbines.

A good frequency estimation algorithm shall be both fast, accurate and robust. The driving force for research has been to improve all these demands simultaneously.

The blackout in 1983 showed the importance of reliable frequency estimation algorithms. At severe disturbances, under-frequency relays are used to disconnect Swedish nuclear power stations from the grid. The relays in operation 1983 were neither designed, nor tuned correctly.

This contributed to the major Nordel blackout in 1983. It was later found that the algorithm used in the relays had problems to estimate low frequency in combination with decreasing voltage amplitude. New relays with better frequency estimation algorithms had to be installed. This example shows the need for research to gain deeper understanding of frequency estimation algorithms.

3.2 Definition of Instantaneous Frequency

This section presents definitions of instantaneous frequency (IF), instantaneous amplitude (IA) and instantaneous phase (IP). The definitions are well established in signal processing, see [2-5]. Given a real signal $f(t)$, we define a complex signal $z(t)$

$$z(t) = f(t) + jH\left[f(t)\right] = a(t)e^{j\phi(t)} \tag{1}$$

where H is the Hilbert transform (HT) defined as

$$H\left[f(t)\right] = p.v.\frac{1}{\pi}\int_{-\infty}^{\infty}\frac{f(t-\tau)}{\tau}d\tau\,. \tag{2}$$

The notation *p.v.* stands for Cauchy principal value, see [4.13]. The instantaneous phase (IP) is defined as

$$IP(t) = \phi(t) = \arg z(t)\,. \tag{3}$$

The instantaneous amplitude (IA) is defined as

$$IA(t) = a(t) = \left|z(t)\right|. \tag{4}$$

The instantaneous frequency (IF_f) in Hz is defined as

$$IF_f(t) = \frac{1}{2\pi}\frac{d}{dt}\left[\arg z(t)\right]. \tag{5}$$

The instantaneous frequency (IF_ω) in rad/s is defined as

$$IF_\omega(t) = \frac{d}{dt}\left[\arg z(t)\right]. \tag{6}$$

This gives unique definitions, but whether or not it corresponds to any physical reality is another question. A discussion on interpretation of IF is found in [6]. Consider the signal

$$s(t) = a(t)\cos\phi(t) \tag{7}$$

with

$$a(t) = \cos(2\pi f_1 t) \text{ and } \phi(t) = 2\pi f_2 t\,. \tag{8}$$

Under what conditions does the definition of instantaneous frequency generate a correct physical interpretation? That is

$$a(t)\cos\phi(t) + jH\left[a(t)\cos\phi(t)\right] = a(t)e^{j\phi(t)} \tag{9}$$

This is true if the spectrum for the amplitude lies in the region $|f| < f_0$ and the spectrum for the phase exists only outside this region. Thus, the signal amplitude $a(t)$ and phase $\phi(t)$ may only be considered independently if the spectra of $a(t)$ and $\phi(t)$ are separated in frequency.

3.3 Some Examples

Some examples are given here with signals that are commonly used in signal processing. The following notations are used. Let *f(t)* be a time signal, then *H*[*f(t)*] is the Hilbert transform and *F*[*f(t)*] is the Fourier transform of *f(t),*

$$F(\omega) = F\left[f(t)\right] = \int_{-\infty}^{\infty} f(t)\, e^{-j\omega t}\, dt \tag{10}$$

From reference [7] and [8] we find the relations in Table 1.

$f(t)$	$H(\tau) = H\left[f(t)\right]$	$F(\omega) = F\left[f(t)\right]$
$\sin(\omega_0 t)$	$\cos(\omega_0 \tau)$	$j\frac{1}{2}[\delta(\omega+\omega_0) - \delta(\omega-\omega_0)]$
$\cos(\omega_0 t)$	$-\sin(\omega_0 \tau)$	$\frac{1}{2}[\delta(\omega+\omega_0) + \delta(\omega-\omega_0)]$
$\mathrm{sinc}(\frac{\omega_0 t}{\pi}) = \frac{\sin(\omega_0 t)}{\omega_0 t}$	$\frac{\cos(\omega_0 \tau) - 1}{\omega_0 \tau}$	$\frac{\pi}{\omega_0}$ for $\lvert\omega\rvert < \omega_0$ 0 otherwise
$\mathrm{rect}(at) = \begin{cases} 1 \text{ for } \lvert t\rvert < \frac{1}{2a} \\ 0 \text{ otherwise} \end{cases}$	$\frac{1}{\pi}\ln\left\lvert\frac{\frac{1}{2a} - \tau}{-\frac{1}{2a} - \tau}\right\rvert$	$\frac{1}{a}\frac{\sin(\frac{\omega}{2a})}{(\frac{\omega}{2a})}$

Table 1. Transforms for some standard signals, where ω_0>0.

The Cosine Signal

This first example is trivial but illustrates the concept of IF. Consider the signal

$$f(t) = \cos t \,. \tag{11}$$

The table shows that the Hilbert transform of $f(t)$ is $H\left[f(t)\right] = -\sin t$. The complex signal becomes $z(t) = \cos t - j \sin t$. The instantaneous amplitude is

$$IA(t) = \left|z(t)\right| = 1 \,. \tag{12}$$

The instantaneous phase becomes

$$IP(t) = \phi(t) = \arg z(t) = -\arctan(\frac{\sin t}{\cos t}) = -t \,. \tag{13}$$

The absolute value of the instantaneous frequency becomes

$$\left|IF_{\omega}(t)\right| = \left|\frac{d}{dt} \arg z(t)\right| = 1 \,. \tag{14}$$

The results correspond with our expectations. This trivial example shows that the definitions give meaningful results for a sinusoidal signal.

The "Sinc" Signal

The second example illustrates how the "sinc" signal is treated. Consider the signal

$$f(t) = \frac{\sin t}{t} \tag{15}$$

which is shown in Figure 1 below.

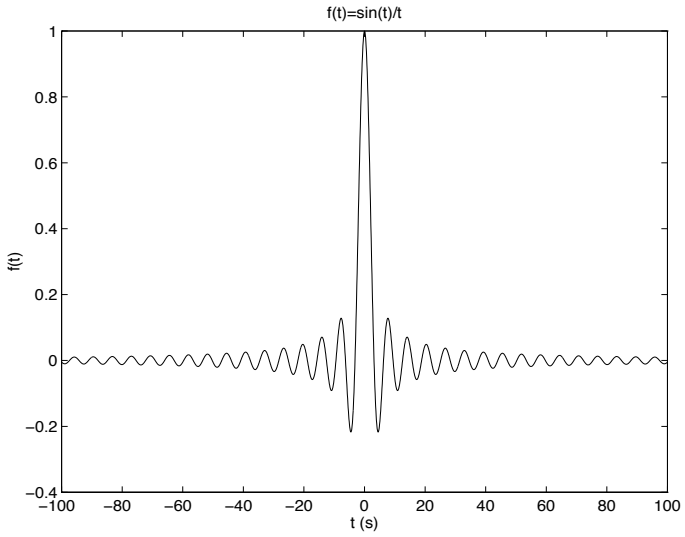

Figure 1. The "sinc" signal.

Table 1 shows that the Hilbert transform of $f(t)$ is

$$H\left[f(t)\right] = \frac{\cos t - 1}{t}. \tag{16}$$

The complex signal becomes

$$z(t) = \frac{\sin t}{t} + j\frac{\cos t - 1}{t}. \tag{17}$$

The instantaneous amplitude becomes

$$IA(t) = \left|z(t)\right| = \frac{\sqrt{2\,(1-\cos t)}}{\left|t\right|} \tag{18}$$

and is shown in Figure 2 below

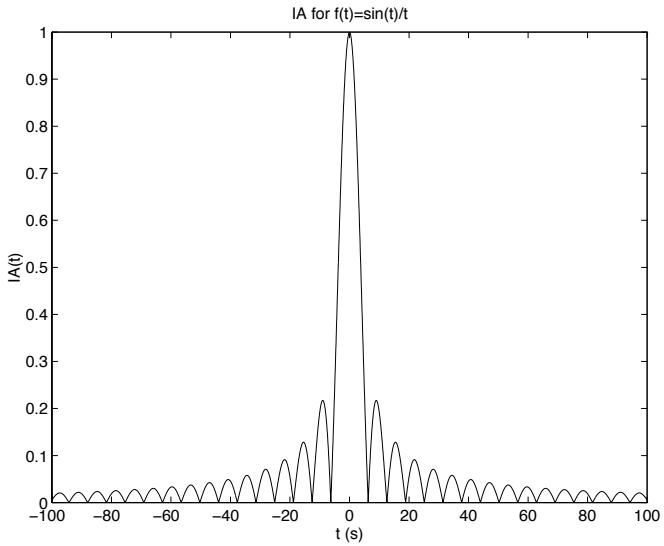

Figure 2. Instantaneous amplitude for the "sinc" signal.

The instantaneous phase becomes

$$IP(t) = \arg z(t) = \arctan(\frac{\cos t - 1}{\sin t}). \tag{19}$$

Taking the derivative of the phase gives the instantaneous frequency

$$\left|IF_{\omega}(t)\right| = \left|\frac{d}{dt}\arg z(t)\right| = \ldots = \frac{1}{2} \text{ rad / s}. \tag{20}$$

We now look at the magnitude of the Fourier transform, often called the spectrum. From the table above we see that $\left|F(\omega)\right|$ is 1 for $\left|\omega\right| < 1$ which is illustrated in Figure 3.

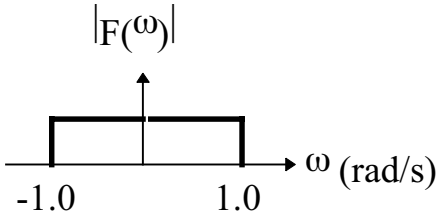

Figure 3. Spectrum for the "sinc" signal.

In this example, we see that the spectrum contains all frequencies between 0 and 1 rad/s. In this case, the IF is independent of time and has a fixed value of 0.50. We note that this value is the mean value of the spectrum, taken for positive ω. We clearly see that the IA is a function of time. With these definitions, all the variation in the time signal is captured in the variation of the instantaneous amplitude. In contrast, the IF becomes constant.

The "Rect" Signal

This example illustrates how the "rect" signal is treated. Consider the signal,

$$f(t) = \begin{cases} 1 \text{ for } |t| < \dfrac{1}{2} \\ 0 \text{ otherwise} \end{cases} \tag{21}$$

shown in Figure 4.

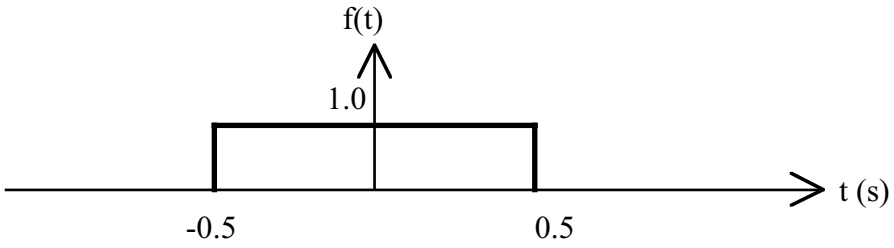

Figure 4. The "rect" signal.

Table 1 gives that the Hilbert transform of $f(t)$ is

$$H\left[f(t)\right] = \frac{1}{\pi}\ln\left|\frac{0.5-t}{-0.5-t}\right| \quad \text{for } |t| \neq 0.5. \tag{22}$$

The complex signal becomes

$$z(t) = f(t) + j\frac{1}{\pi}\ln\left|\frac{0.5-t}{-0.5-t}\right|, \tag{23}$$

that is

$$z(t) = \begin{cases} 1 + j\frac{1}{\pi}\ln\left(\frac{0.5-t}{0.5+t}\right) & \text{for } |t| < 0.5 \\ j\frac{1}{\pi}\ln\left|\frac{0.5-t}{-0.5-t}\right| & \text{for } |t| > 0.5 \end{cases}. \tag{24}$$

The instantaneous amplitude becomes

$$IA(t) = \begin{cases} \sqrt{1 + \left(\frac{1}{\pi}\ln\left(\frac{0.5-t}{0.5+t}\right)\right)^2} & \text{for } |t| < 0.5 \\ \frac{1}{\pi}\ln\left|\frac{0.5-t}{-0.5-t}\right| & \text{for } |t| > 0.5 \end{cases} \tag{25}$$

The amplitude is shown in Figure 5 below. Note that the amplitude is discontinuous for $|t| = 0.5$ and is not plotted for this value. The limit value is unbounded and the amplitude goes to infinity as $|t| \to 0.5$.

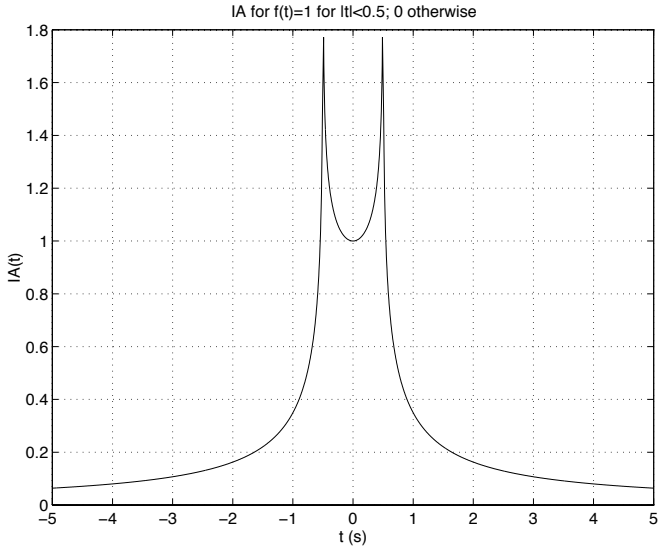

Figure 5. Instantaneous amplitude for the "rect" signal.

The instantaneous phase becomes

$$IP(t) = \arg z(t) = \begin{cases} \arctan\left(\frac{1}{\pi}\ln\frac{0.5-t}{0.5+t}\right) & \text{for } |t| < 0.5 \\ -\frac{\pi}{2} & \text{for } t > 0.5 \\ +\frac{\pi}{2} & \text{for } t < 0.5 \end{cases} \tag{26}$$

For $|t| < 0.5$ we take the derivative of the phase that gives

$$\left|IF_{\omega}(t)\right| = \left|\frac{d}{dt}\arg z(t)\right| = \ldots = \frac{1}{1+\left[\frac{1}{\pi}\ln\frac{0.5\text{-}t}{0.5+t}\right]^2}\cdot\frac{\frac{1}{\pi}}{\frac{0.5\text{-}t}{0.5+t}}\cdot\frac{-1}{(0.5+t)^2}$$

$$= \frac{1}{1+\left[\frac{1}{\pi}\ln\frac{0.5\text{-}t}{0.5+t}\right]^2}\cdot\frac{1}{\pi}\cdot\frac{1}{t^2-0.25} \qquad (27)$$

and we have

$$\left|IF_{\omega}(t)\right| = \begin{cases} \dfrac{1}{1+\left[\frac{1}{\pi}\ln\frac{0.5\text{-}t}{0.5+t}\right]^2}\cdot\dfrac{1}{\pi}\cdot\dfrac{1}{t^2-0.25} & \text{for } |t| < 0.5 \\ 0 \quad \text{otherwise} \end{cases} \qquad (28)$$

Figure 6 shows the instantaneous frequency.

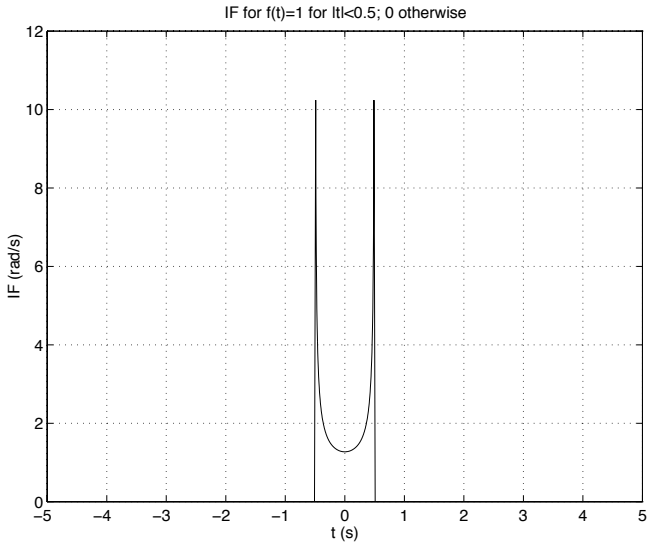

Figure 6. The instantaneous frequency for the "rect" signal.

We continue with the magnitude of the Fourier transform, often called the spectrum. Table 1 shows that the spectrum is

$$\left|F(\omega)\right| = \frac{\left|\sin\frac{\omega}{2}\right|}{\frac{\omega}{2}}$$

that is, a "sinc". Figure 7 below shows the spectrum.

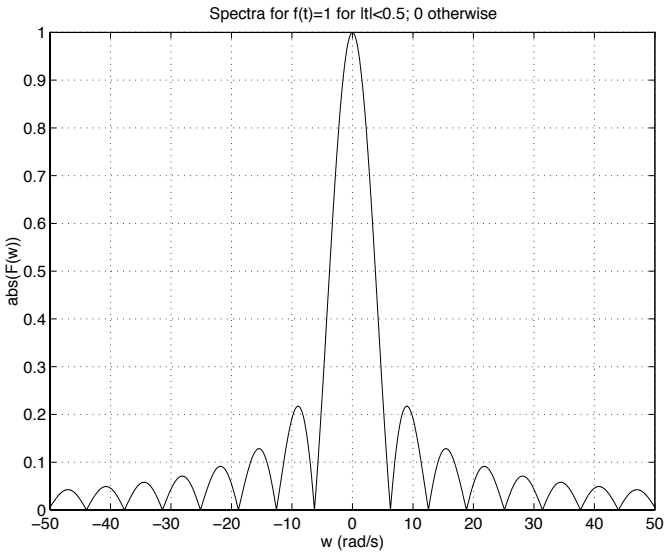

Figure 7. Spectrum for the "rect" signal

In this example, we see that the spectrum contains almost all frequencies between zero and infinity, except at points where $\omega = 2\pi k$ for $k = 1,2,3\ldots$. In this case, both the IF and the IA vary with time and go to very high values as $|t| \to 0.5$. For this signal the time variation in the signal $f(t)$ is captured both in variation in the IA and in the IF.

3.4 Frequency Estimation in Power Systems

Here is a brief discussion about frequency estimation in power systems. Many methods for frequency estimation in power systems are based on the same idea as instantaneous frequency in signal processing. This is illustrated by some examples. A more extensive literature survey is given in [1]. The general procedure for frequency estimation is:

1. Use measurements to calculate two quantities that are orthogonal in the sense that they have a phase difference of 90 degrees.
2. Interpret the two orthogonal quantities as the real and imaginary part of a complex number. Convert the complex number to polar form with an amplitude and a phase.
3. The frequency is estimated as the change in phase, i.e., the derivative of the phase.

In the definition (1), used in signal processing, the purpose of the Hilbert transform is to give a 90 degree phase shift of the signal *f(t)*. References [9-11] show how to implement the Hilbert transform as a discrete filter that gives 90 degrees phase shift and approximately unity gain over the frequency range of interest. The drawback with the discrete Hilbert transform filter is that it introduces a phase lag.

The paper [12] has become a standard reference for frequency estimation in power systems. Here, the Discrete Fourier Transform is used to create a complex signal. The deviation from nominal frequency is calculated as a change in phase angle. This fits into the general procedure above.

In [13], the αβ-components are used to get two orthogonal signals. The αβ-components are simply a linear combination of the three phase quantities. One advantage is that the calculation does not introduce any phase shift. Another advantage is that, since no filters are used, the gain of the two components are not affected by varying frequency such as in [15]. This method is excellent to measured frequency within a broader interval, say from 10 Hz up to 100 Hz. One typical application is to measure speed (frequency) during startup, or load rejection, of a gas turbine. The method's drawbacks are that all three phases are used and that the system needs to be symmetric.

The paper [14] describes an extensive piece of work that was done to find a suitable frequency estimation method for the French defence plan against loss of synchronism. The methods presented in the papers fit into the general procedure outlined above. The paper also discusses discrete Hilbert transform filter as an alternative to get the 90 degrees phase shift.

Reference [15] is yet another recent paper that uses the above procedure. The method uses only one phase quantity as input signal. Finite impulse filters (FIR), based on sine and cosine impulse response, are used to get two orthogonal components. One drawback with the method is that the filter introduces delays. Secondly, the two filters only have equal gains at the nominal frequency. The authors suggest using the estimated frequency to adjust the filter gains. This patch is called an adaptive feedback loop. The main advantage with this method is the simplicity. It is easy to measure one signal and implement the FIR filters.

For a power engineer, it is feasible to implement FIR filter with sine and cosine impulse response. Design and implementation of discrete Hilbert transform filter requires more knowledge of signal processing and is beyond reach for many power engineers. The authors point out that the combined use of two filters—one with antisymmetric and one with symmetric impulse response—ensures that the filter outputs differ by 90 degrees for all input frequencies. The remaining problem is to get identical filter gains for all frequencies. Discrete Hilbert transform filters address exactly this problem—how to make a filter that gives 90 degrees phase shift and have unity gain for all frequencies.

My contribution in Appendix B presents a method for frequency estimation in power system by demodulation of two complex signals.

The method has been previously published [13], but not explored to its potential. In power system analysis, the $\alpha\beta$-transform is used to convert three phase quantities to a complex quantity where the real part is the in-phase component and the imaginary part is the quadrature component. This complex signal is demodulated with a known complex phasor rotating in opposite direction to the input. The advantage of this method is that the demodulation does not introduce a double frequency component. For signals with high signal to noise ratio, the filtering demand for the double frequency component can often limit the speed of the frequency estimator. Hence, the method can improve fast frequency estimation of signals with good noise properties. The method loses its benefits for noisy signals, where the filter design is governed by the demand to filter harmonics and white noise. The paper presents four examples to illustrate the strengths and weaknesses of the method.

One possible conclusion is that some of the questions that arise in power systems are just special cases of general problems that have already been addressed in signal processing. It is just a matter of finding the relevant results and picking out the useful parts.

3.5 References

[1] Akke, M., "A Literature Survey of Frequency Estimation Methods," Report TEIE-7121, Department of Industrial Electrical Engineering and Automation, Lund Institute of Technology, Lund, Sweden, March 1997.

[2] Boashash, B., "Estimating and Interpreting the Instantaneous Frequency of a Signal - Part 1: Fundamentals," *Proceedings of IEEE*, Vol. 80, No. 4, April 1992, pp. 520-538.

[3] Boashash, B., "Estimating and Interpreting the Instantaneous Frequency of a Signal - Part 2: Algorithms and Application," *Proceedings of IEEE*, Vol. 80, No. 4, April 1992, pp. 540-568.

[4] Boashash, B., "Time Frequency Signal Analysis—Past, Present and Future Trends," To appear in *Control and Dynamic Systems*, ed. by C. T. Leondes, Academic Press, USA, 1994.

[5] Boashash, B., "Time Frequency Signal Analysis," reprint from *Advances in Spectrum Estimation*, pp. 418-517, edited by S. Haykin, Prentice-Hall, USA, 1990.

[6] Mandel, L., "Interpretation of Instantaneous Frequency," *Amer. J. Phys.*, Vol. 42, 1974, pp. 840-846.

[7] Råde, L. and Westergren, B., *Beta—Mathematics Handbook*, Studentlitteratur, Sweden, 1990.

[8] Erdalyi, A. et al., *Tables of Integral Transforms, Vol. 1-3*, Bateman Manuscript Project, California Institute of Technology, McGraw-Hill, New York, USA, 1954.

[9] Cooklev, T. and Nishihara, A., "Maximally flat FIR Hilbert transformers," *International Journal of Circuit Theory and Applications*, Vol. 21, No. 6, Nov-Dec 1993, pp. 563-570.

[10] Gold, B., Oppenheim, A. V., and Rader, C. M., "Theory and Implementation of the Discrete Hilbert Transform," *Proc. of Symp. Computer Processing in Communications*, Vol. 19, Polytechnic Press, New York, USA, 1970.

[11] Rabiner, L.R., and Schafer, R. W., "On the Behavior of Minimax FIR Digital Hilbert Transformer," *Bell System Technical Journal*, Vol. 53, No. 2, February 1974, pp. 361-388.

[12] Phadke, A.G., Thorp, J.S. and Adamiak, M.G., "A New Measurement Technique for Tracing Voltage Phasors, Local System Frequency, and Rate of Change of Frequency," *IEEE Transaction on Power Apparatus and Systems*, Vol. PAS-102, No. 5, May 1983, pp. 1025-1038.

[13] Eckhardt, V., Hippe, P. and Hosemann, G., "Dynamic Measuring of Frequency and Frequency Oscillations in Multiphase Power Systems," *IEEE Transaction on Power Delivery*, Vol. 4, No. 1, January 1989, pp. 95-102.

[14] Denys, P., Counan, C., Hossenlopp, L. and Holweck, C., "Measurement of Voltage Phase for the French Future Defence Plan Against Losses of Synchronism," *IEEE Transaction on Power Delivery*, Vol. 7, No. 1, January 1992, pp. 62–69.

[15] Moore, P.J. et al., "New Numeric Technique for High-Speed Evaluation of Power System Frequency," *IEE Proceedings of Generation, Transmission and Distribution*, Vol. 141, No. 5, September 1994, pp. 529–536.

Chapter 4

Computer Relaying

Computer relaying is presented in this chapter. The two papers in Appendix C and D, present the author's contribution. The chapter starts with an introduction that leads to the main theme of this chapter—computer relaying for distance protection of transmission lines. The last section presents statistical calculations.

4.1 Introduction

Protection

Even if the non-specialist may think about protection in very diverse areas, it has a special and concise meaning in power systems. Power system protection can be divided into two main categories, system wide protection and protection of objects.

System wide protection is a novel concept that aims to detect and prevent system failures such as voltage collapse, power oscillations and loss of synchronism. In the following we mainly deal with local protection.

Protection of objects have been an integrated part of the power system for nearly a hundred years. The main task is to protect one object such as a transformer or an overhead line. Even though the relay protects a single object, a malfunction can affect the overall integrity of the power system. The primary task of the relay protection is to detect a fault within the protected zone, and then give a trip signal to the appropriate breaker or breakers. In addition to the relay, the other parts of the fault clearance system are voltage and current transformers, DC-supply, communication channels, and some switching devices (breakers or disconnectors) [7]. Relay protection must fulfill demands and requirements from several different interest groups. In Sweden the following have to be considered:

- the Swedish Electricity Act from 1902;
- regulations for power installations;
- demands from telephone companies and their customers;
- demands from the owner of the power system;

- demands from the power system operator;
- safety requirement for maintenance work.

The apparatus protected by the relay is called the protected object. Different types of power system components, for example a transmission line and a generator, have totally different operation principles. There can also be a significant difference in price. Therefore, relay protection is often structured into the following types:

- distribution line protection;
- transmission line protection;
- rotating machinery protection;
- transformer protection;
- bus-bar protection;
- reactor protection;
- capacitor protection;
- HVDC-protection;
- system protection—wide area protection.

In transmission systems the relay protection of overhead lines are especially important. Too long fault clearing time can cause transient instability. An unwanted trip of a line during a disturbance, can cause a voltage collapse or undamped power oscillations. In North American literature [6], the relays for transmission lines are further categorised as:

- non-pilot over-current protection of transmission lines;
- non-pilot distance protection of transmission lines;
- pilot protection of transmission lines.

The rest of this chapter deals with the second item above, that is, non-pilot distance protection of transmission lines. In particular, we focus on digital algorithms suitable for computer relaying.

Computer Relaying

The development of computer relaying has been governed by the access to reliable and low cost microcomputer technology. The development started in the 1960s with research and feasibility studies. The driving forces were primarily engineering curiosity and the potential of new academic research. At that time computer power was expensive and digital relays did not spread until the prices of microprocessors dropped. Rockefeller was a pioneer in the field and published one of the first papers on computer relaying [1]. The textbook [6] contains a general introduction to relaying

in power systems with emphasis on North American practice. The two textbooks [2] and [3] present computer relaying and list also many relevant references. The two volumes of IEEE collection of papers [4, 5] are also good sources of original material.

Global Positioning System (GPS)

Global Positioning System (GPS) technology has the potential to cause the largest paradigm shift in relaying since the introduction of microcomputers. From the beginning GPS was a military system for navigation. Today it is a widespread system with many civilian uses. The main use is still navigation, but many new applications have evolved. One novel use of GPS is to time synchronize measurement in power systems. The authors to [14-22] have played key roles in the development of phase measurement units (PMU). There are turnkey PMUs on the market, but due to low production volumes, prices are still high. When production volume increases, prices are expected to drop. Some typical uses of one or several PMUs are:

- to improve, or even replace, state estimators [14];
- for monitoring of power system disturbances;
- for system wide protection and control schemes [11, 22].

So far we have just scratched the surface of all possible uses of synchronized clocks. It is not far fetched to believe that we have only seen the beginning of a technology that can revolutionize computer relaying and even power system control. For example, with GPS providing synchronized clocks and fiber optics providing fast signal transmission, it would be feasible to do differential protection of objects that are distributed over a large geographical area.

4.2 Digital Algorithms for Transmission Line Protection

This section deals with digital algorithms for transmission line protection, also known as digital distance protection. We are interested in relays where only local quantities are used. Differential line relays and relays using pilot wires are excluded. Algorithms used for digital distance protection are:

- Fourier based algorithms;
- differential equation algorithms;
- traveling wave algorithms.

Many commercial relays are, in one way or another, based on Fourier algorithms. These algorithms are well known and are described in detail in [2], [3]. The paper [8] describes how to use symmetrical components together with Fourier type algorithms to get a so called "full scheme relay". The Fourier algorithms are based on an assumption of the signal, that it is of nominal system frequency and sinusoidal. The algorithm basically filters out the Fourier coefficient for the 50 Hz (or 60 Hz) component of the signal. The main advantages with the algorithm are the reliability and the robustness properties. Another advantage is that it is straightforward to analyze the algorithm. The algorithm requires around one cycle, i. e., 20 ms, to produce accurate results. The relatively long time can be a drawback in applications where fast fault clearing is needed.

In contrast, the differential equation algorithm (DEA) is based on the assumption of a model that is described by a differential equation. Any type of signal that fulfills the equation produces useful estimates of the fault location. The DEA is well described in textbooks such as [2, 3]. However, the zero sequence resistance is missing in the equations in [3]. Therefore [2] is favored as background literature on the DEA.

Transmission relays based on traveling waves is another theme that is described in [9]. The type is not widespread and is more of a special application relay.

Computer Relaying Toolbox

A "Computer Relaying Toolbox" for transmission lines has been implemented in Matlab [10]. It has been used to study the properties of Fourier based algorithms and the DEA. Figure 1 shows the graphical user interface to the toolbox.

Figure 1. The graphical user interface to a computer relaying toolbox for Matlab.

Some of the algorithms in [2] and also the algorithm presented in [8] have been implemented. The toolbox has proved to be very useful in gaining insight into algorithm behavior, and also to test new ideas.

Contribution in Papers

In the two papers in Appendix C and D some improvement to the DEA are suggested. Many of the ideas in the papers originate from work with the

Computer Relaying Toolbox. The DEA is based on the assumption that the dynamics of the power line can be described by a differential equation. Any signal that fulfills the equation can be used to estimate the fault location. Fourier based algorithm assumes a signal of the fundamental frequency. One practical implication is that the DEA can be faster than Fourier based algorithms. However, relay implementations of the DEA have not been successful. It has been reported that the algorithm occasionally magnifies noise.

The first paper explains the magnification of noise in terms of a singular equation system. A singular equation system gives extremely poor estimates of the fault location. Median filter is suggested to eliminate these poor estimates.

The second paper suggests the following improvements to the DEA:

- a fault classification scheme for DEA that incorporates the equations for the different fault types into a unified fault estimator;
- speed improvements for three-phase faults, by using two equations with orthogonal quantities;
- improved filtering of the DEA estimates.

Simulation results indicate that the nominal operation time for a three-phase fault is 5-7 ms.

The next section takes a statistical view on fault estimation that yields some general results that can look rather surprising.

4.3 Stochastic Analysis of Fault Locators

In this section we further develop the ideas in the papers in Appendix C and D. Reference [12] has been used for the statistical background, but most undergraduate textbooks in statistic could be used. An estimation of the fault location k often involves a calculation of a ratio such as

$$k = \frac{X_1}{X_2}. \tag{1}$$

If the variables X_1 and X_2 are free from noise everything is fine. But if X_1, and even worse X_2 are contaminated with noise the situation gets complicated. Here we will present an analysis using statistics. Assume that X_1 and X_2 are stochastic variables that can be described by two normal distributions, that is

$$X_1 \in N(m_1, \sigma_1) \text{ and } X_2 \in N(m_2, \sigma_2) \tag{2}$$

where m is the expected value and σ is the standard deviation for a normal distribution. The probability density function (pdf) for a normal distribution is,

$$f_X(x) = \frac{1}{\sigma\sqrt{2\pi}} \exp(-\frac{(x-m)^2}{2\sigma^2}). \quad (3)$$

If the noise level is low, that is σ_1 and σ_2 are close to zero, we have

$$k \approx \frac{m_1}{m_2}. \quad (4)$$

What happens if the standard deviation σ is around the same magnitude as the expected value *m*? The division with X_2 causes problem. We focus on the probability that X_2 becomes zero and ruins the division. To shed some light on the problem we concentrate on the properties of the stochastic variable

$$Y = \frac{1}{X} \text{ where } X \in N(m,\sigma). \quad (5)$$

Expected Value of 1/X

The notation $E[\ ]$ is used for expected value. We are interested in $E[Y]$ where $Y = \frac{1}{X}$ and $X \in N(m,\sigma)$. By intuition, or by Poissons formula [12], we might expect that

$$E[Y] \approx \frac{1}{m} \text{ if } \sigma << m. \quad (6)$$

Yet another option would be to use Jensen's lemma [23] that says that

$$E[Y(X)] \geq Y(E[X])$$

if *Y* is a convex function of the stochastic variable *X*. We have the function *Y=1/X* that is convex only if *x>0*. The lemma is not directly applicable and to apply it we need to reformulate the problem. For our problem, the lemma is not so useful.

To calculate the expected value we have to solve

$$E\left[\frac{1}{X}\right] = \int_{-\infty}^{\infty} \frac{1}{x} f_X(x)\,dx = \int_{-\infty}^{\infty} \frac{1}{x} \frac{1}{\sigma\sqrt{2\pi}} \exp(-\frac{(x-m)^2}{2\sigma^2})dx. \quad (7)$$

The integral has inspired some mental efforts. Despite consultation of mathematics references, a primitive function has not been found. Thus, numerical integration has to be used. The integral is complicated to solve numerically because of a discontinuity at zero and the infinite integration

limits. The equality from Appendix E is used to eliminate these difficulties. We use the equality to rewrite the integral as

$$E\left[\frac{1}{X}\right] = \frac{1}{\sigma}\exp\left[-\frac{1}{2}\left(\frac{m}{\sigma}\right)^2\right]\int_0^{m/\sigma}\exp\left(\frac{x^2}{2}\right)dx\,. \tag{8}$$

The new integral is both continuous and has bounded integration limits. The equality used is believed to be an original contribution by the author. The mathematically interested reader is referred to Appendix E for a proof. Now it is straightforward to use numeric integration to solve the new integral. Assume that m has been normalized to 1 per unit (p.u.) by selecting a suitable base and that σ is expressed in this base. Figure 2 shows the expected value $E[1/X]$ as a function of σ.

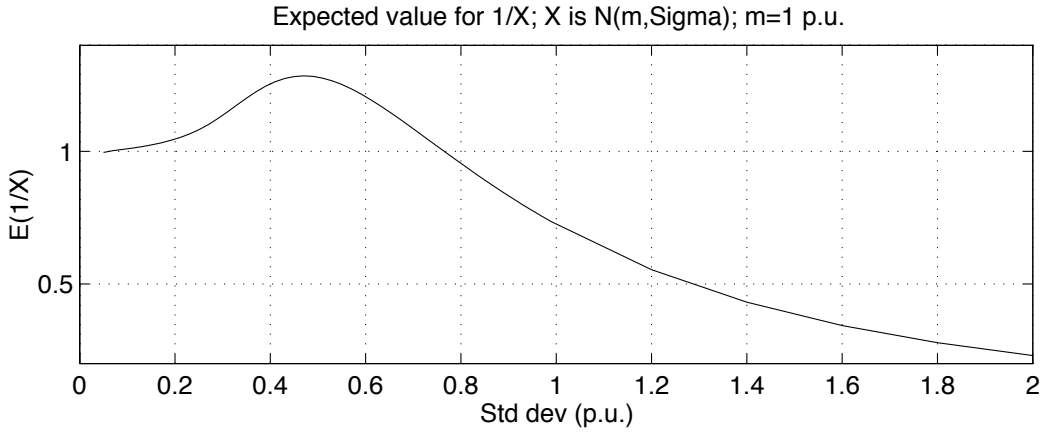

Figure 2. Expected value of 1/X as a function of σ. The stochastic variable X is normally distributed with expected value *m=1* and standard deviation σ.

The following observations are made. The expected value $1/X \rightarrow 1/m=1$ if, and only if, $\sigma \rightarrow 0$. If the standard deviation goes to large values, the expected value tends to zero. Intuitively this can be understood as the probability density function is spread out, taking both positive and negative values. The expected value tends to zero as the distribution tends to be symmetric around zero. The interesting part of Figure 2 is when the standard deviation has moderate values, neither too small nor too large. We see that the expected value is somewhat larger than $1/m=1$. This is important. In terms of estimation we get a biased estimate. The only way to get an unbiased estimate is to secure a small standard deviation in X before calculating $1/X$. Low pass filtering before calculating $1/X$ is a good method of reducing the bias.

Assume that we have a stochastic variable X with $m=1$ and $\sigma = 0.5$. Without any filtering, Figure 2 shows that $\sigma = 0.5$, corresponding to an expected value of $1/X$ around 1.28. An average filter of order 16, reduces the standard deviation by a factor 4. Thus, the standard deviation is

reduced to 0.125 by the filter. Figure 2 shows that the expected value of *1/X* becomes 1.01.

We find that without filtering the fault location is biased by more than 25%. A simple average filter reduces the bias to 1%. Note that any low pass filtering performed after the division does not affect the bias. We still get the error due to the bias. The lesson learnt is that it is very important to have a standard deviation that is low before the division is made, otherwise errors are introduced. A rule of thumb is that the standard deviation should be less than 20% of the expected value to get an estimate that is practically unbiased.

Variance and Probability for Zero Division

It would have been satisfying to be able to calculate the variance (standard deviation) of *1/X*. However it is not possible to the do the same type of calculation as for the expected value. This is due to the fact that the variance does not exist, or in other words, is unbounded. To calculate the variance we have to solve the integral

$$E\left[\frac{1}{X^2}\right] = \int_{-\infty}^{\infty} \frac{1}{x^2} f_X(x)\,dx = \int_{-\infty}^{\infty} \frac{1}{x^2} \frac{1}{\sigma\sqrt{2\pi}} \exp\left(-\frac{(x-m)^2}{2\sigma^2}\right) dx\,. \qquad (9)$$

To the best of my knowledge, this is not solvable. Numerical integration has been used to verify that the integral diverge as the integration step becomes smaller.

Another way of calculating the probability of a zero division is to use a somewhat practical approach. The problem of zero division occurs if the value x of the stochastic variable X is very close to zero. The meaning of "very close to zero" can be seen from an implementation point of view. Assume a 12-bit AD converter with 4096 levels and a range of the converter from -2 to +2 Volt, so that the smallest level is around 1 mV. The interval that is truncated to zero is then around 1 mV. Thus the probability of getting a zero can be approximated by the length of the zero interval multiplied by the pdf at zero. We can estimate the probability of getting a zero division as a function of the standard deviation. We assume that the interval from -ε/2 to ε/2 is truncated to zero. Thus the probability is

$$P(\text{zero division}) \approx P\left(-\tfrac{\varepsilon}{2} < X < \tfrac{\varepsilon}{2}\right) =$$

$$= \int_{-\frac{\varepsilon}{2}}^{\frac{\varepsilon}{2}} f_X(x)\,dx \approx \varepsilon\, f_X(0) = \frac{\varepsilon}{\sigma\sqrt{2\pi}} \exp\left(-\frac{m^2}{2\sigma^2}\right) \qquad (10)$$

In the same way as above we assume that *m=1* p.u.. Matlab has been used to calculate the probability of a zero division. Instead of presenting the probability, which is a very small number, the inverse is presented. The inverse can be interpreted as the expected number of samples before a zero division is obtained. It should be related to the concept Mean Time Between Failure (MTBF) that is often used as a reliability measure. Figure 3 shows the result.

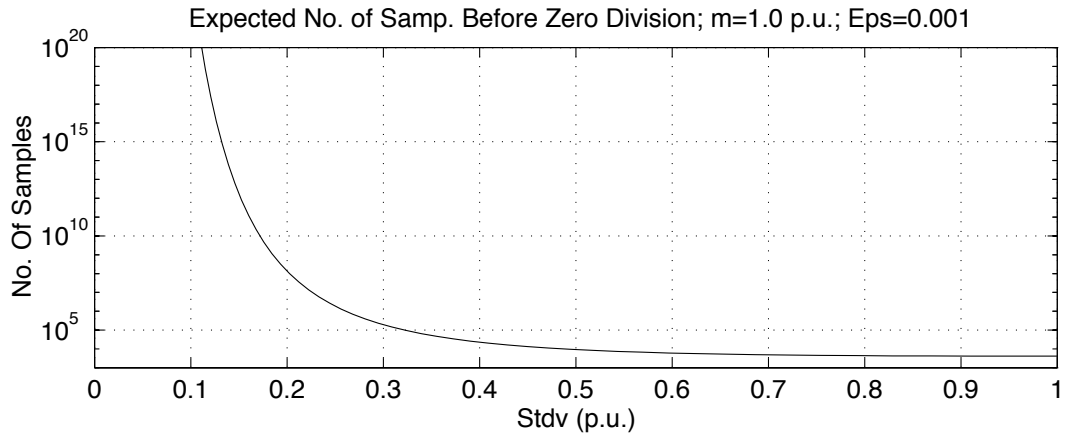

Figure 3. Expected number of samples before zero division for 1/X as a function of the standard deviation σ. The stochastic variable X is normally distributed with expected value *m=1* and standard deviation σ. The length of the interval that is truncated to zero is ε=0.001.

From Figure 3 the following observations can be made. The probability for zero division is of practical concern when the standard deviation is larger than 0.3-0.4 p.u. We also note that the change in probability is highly non-linear. So a low order filter before the division can drastically reduce the probability of a zero division. For example, if the standard deviation is 0.5 p.u., an average filter of length 16 would reduce the standard deviation by a factor 4, so it would be 0.125 after filtering. The expected number of samples before zero division would rise from 10^4 to 10^{18}. Assume that each time the relay operates it uses 1000 samples. Without filtering we would expect that every tenth operation would give a zero division and possible malfunction. In contrast, a short average filter could boost the expected number of operations before a zero division is obtained to 10^{15} operations.

Consequences for Calculation in the DEA

To get unbiased estimates and a low probability for zero division it is necessary to keep the noise level low. If the noise can be modeled as normally distributed white noise, a rule of thumb is to keep the standard deviation less than 0.2 of the expected value. One way to reduce the noise levels is to filter the numerator and the denominator separately before the

division is made. Another question is how relevant the statistical model is. At least it makes us realize that division can cause problems and helps us to gain some insight.

4.4 References

[1] Rockefeller, G. D., "Fault Protection with a Digital Computer," *IEEE Transaction on Power Apparatus and Systems*, Vol. 88, No. 4, April 1969, pp. 438-461.

[2] Phadke, A. G. and Thorp, J. S., *Computer Relaying for Power Systems,* Research Studies Press Ltd., Taunton, Somerset, England, 1994.

[3] Johns, A. T. and Salman, S. K., *Digital Protection for Power Systems,* Peter Peregrinus Ltd. on behalf of IEE, London, England, 1995.

[4] Horowitz, S. H. (editor), *Protective Relaying for Power Systems*, IEEE Press, USA, 1980. (ISBN 0-87942-140-1)

[5] Horowitz, S. H. (editor), *Protective Relaying for Power Systems II*, IEEE Press, USA, 1992. (ISBN 0-7803-0413-6)

[6] Horowitz, S. H. and Phadke, A. G., *Power System Relaying*, Research Studies Press Ltd., Taunton, Somerset, England, 1995.

[7] Lindahl, S., Fault Clearing in T̤ransmission System, (in Swedish), Sydkraft Report PDS-8810-09, Malmo, Sweden, February, 1991.

[8] Phadke, A. G., Hlibka, T. and Ibrahim, M., "Fundamental Basis for Distance Relaying with Symmetrical Components," *IEEE Transaction on Power Apparatus Systems*, Vol. 96, No. 2, March/April 1977, pp. 635-646.

[9] Chamia, M. and Liberman, S., "Ultra High Speed Relay for EHV/UHV Transmission Lines—Development, Design and Application," *IEEE Transaction on Power System Apparatus and Systems*, Vol. PAS-97, November/December 1978, pp. 2104-2112.

[10] *Matlab-Reference Guide*, The MathWorks, Inc., Natick, Mass.

[11] Rovnyak, S. M., Algorithms for Real-Time Transient Stability Prediction in Electric Power Systems, Ph.D. dissertation at School of Electrical Engineering, Cornell University, USA, May 1994.

[12] Blom, G., *Probability Theory with Applications* (in Swedish), Studentlitteratur, Lund, Sweden, 1980.

[13] Saff, E. B., and Snider, A. D., *Fundamentals of Complex Analysis for Mathematics, Science, and Engineering*, Prentice-Hall, Inc. Englewood Cliffs, NJ, USA, 1976.

[14] Phadke, A. G., Thorp, J. S. and Karimi, K. J., "State Estimation with Phasor Measurements," *IEEE Transaction on Power Systems*, Vol. PWRS-1, No. 1, February 1986, pp. 233–241.

[15] Phadke, A.G., "Synchronized Phasor Measurements in Power Systems," *IEEE Computer Applications in Power*, Vol. 6, No. 2, April 1993, pp. 10-15.

[16] Phadke, A.G et al., "Synchronized Sampling and Phasor Measurements for Relaying and Control," *IEEE Transaction on Power Delivery*, Vol. 9, No. 1, January 1994, pp. 442-452.

[17] Thorp, J. S., "Control of Electric Power System Using Real-Time Measurements," *IEEE Control Systems Magazine*, Vol. 9, No. 1, January 1989, pp. 39-45.

[18] Wilson, R. E., "Uses of Precise Time and Frequency in Power Systems," *Proceedings of IEEE*, Vol. 79, No. 7, July 1991, pp. 1009-1018.

[19] Wilson, R. E., "Methods and Uses of Precise Time in Power Systems," *IEEE Transaction on Power Delivery*, Vol. 7, No. 1, January 1992, pp. 126-132.

[20] Wilson, R. E., "PMUs," *IEEE Potentials*, Vol. 13, No. 2, April 1994, pp. 26-28.

[21] Wilson, R. E. and Sterlina, P. S., "GPS Synchronized Power System Phase Angle Measurements," *International Journal of Satellite Communications*, Vol. 12, No. 5, September/October 1994, pp. 499-505.

[22] Stanton, S.E. et al., "Application of Phasor Measurements and Partial Energy Analysis in Stabilizing Large Disturbances," *IEEE Transaction on Power Systems*, Vol.10, No. 1, February 1995, pp. 297-306.

[23] Chung, K. L., *A Course in Probability Theory*, Academic Press, New York, 1974.

Chapter 5

Damping of Power Oscillations by Load Switching—Field Tests at Hemsjo Hydro Power Station

This chapter presents field tests performed at the hydro power station Hemsjo Ovre, the night between 24 and 25 September, 1996. The chapter is descriptive and more technical details are given in [3-4]. The tests were done to investigate if load switching can be used to damp power oscillations. The results show that load switching is an excellent method of damping power oscillations. The method has the potential to become a better and more economic damping method than power system stabilizers (PSS). The chapter starts with an introduction. Section 5.2 describes the setup and the equipment used. Some major results are presented in section 5.3.

5.1 Introduction

Motivation

The electricity market in Sweden was deregulated at the beginning of 1996. This has contributed to the fact that much interest within power companies has turned towards marketing and business. Resources have been reallocated accordingly. Since there have not been any major power oscillations in the Nordic power system during recent years, there have not been any short term economic benefits of studying the problem.

A major disturbance on the first day of 1997 came as a reminder, that it is crucial to keep a very high competence in power system analysis. The disturbance was severe and the Nordic power grid (Nordel) was close to a blackout. The disturbance was triggered by a bus-bar fault that tripped several lines; shortly after the initial disturbance a second line was tripped due to overload. At this point two power nuclear units were connected to the grid by weak radial lines. Power oscillations with growing amplitude followed which caused the two nuclear units Ringhals 1 and 2 to trip. After the trips, the power oscillations were damped out and a frequency

drop followed. Figures 1–3 show the power, voltage and frequency at the receiving end of the radial line.

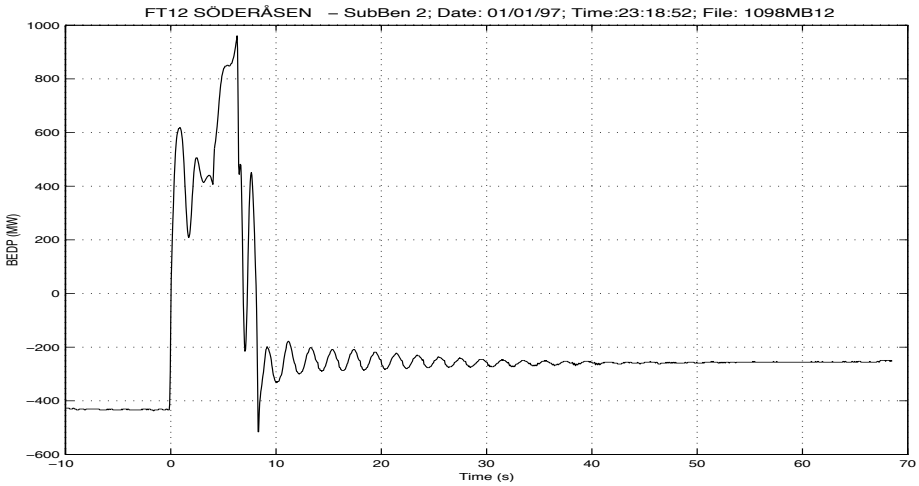

Figure 1. Active power on the 400 kV line from Söderåsen to Breared.

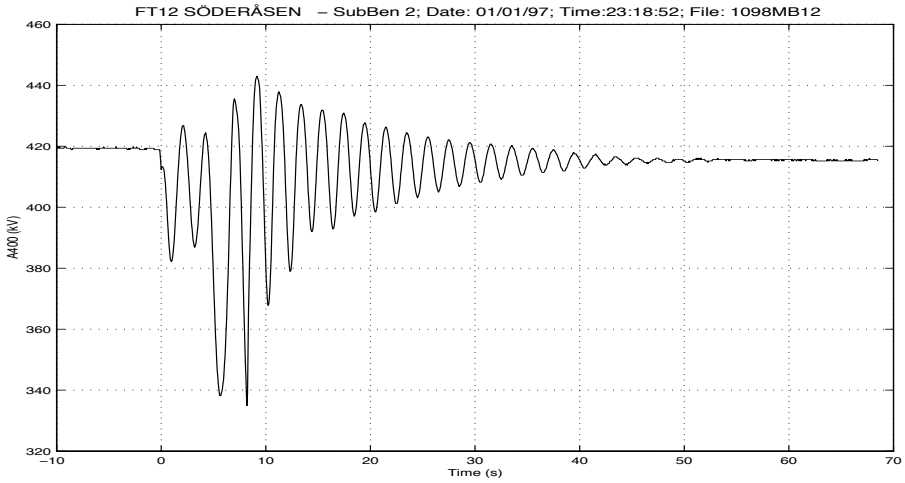

Figure 2. Voltage at the 400 kV substation in Söderåsen.

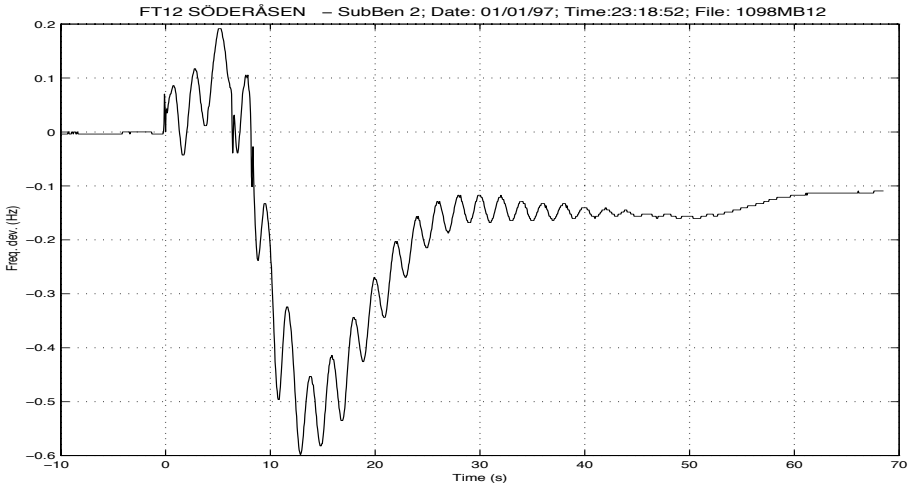

Figure 3. Frequency deviation at the 400 kV substation in Söderåsen.

The event shows that serious disturbances are a reality. The lesson learnt was that power oscillations can jeopardize the operation of power systems.

It also motivates the search for alternatives to improve power system stability.

Power System Stabilizers

Power system stabilizers (PSS) are often applied with the intention of improving system damping. A literature review, see [6-7], shows that a lot of effort has been put into design and tuning methods for power system stabilizers. If not properly tuned the PSS can make things worse, i.e., decrease damping. A dynamic model of the power system is needed to calculate PSS parameters. The field tuning in Sweden has been done to provide good damping for one local mode at one operation point. The PSS performance under model uncertainties or under different operating conditions is not fully understood. The question is complex and has no simple answer. Some recent research on robustness is presented in [8]. Interesting tuning work has been done in Denmark by Torben Østrup, see [9]. Power oscillations of different frequencies have been excited from one generator, while the PSS has been tuned on a neighboring generator.

Damping of Power Oscillations by Load Switching

The idea is to switch a resistive load so it counteracts power oscillations. We used the angle difference between the external net and the generator to control the load switching. The load used was pure resistance without any dynamics and was dedicated for this purpose. One convenient feature of load switching is that very simple models are needed. Therefore the method has the potential to be robust to modeling errors and to varying operation conditions. The engineering work needed for load switching is simpler than for PSS and it is far less complicated to design a load switching system that is robust and simple. The drawback with load switching is the need of additional hardware such as resistive loads and thyristor control. The hardware needed can be reduced if existing equipment can be used. For example, it might be feasible to use electrical heaters normally used for district heating. Then just a new thyristor control unit is needed.

When comparing costs between PSS and load switching, it is important to remember to include all costs, both for the hardware and the engineering work. For PSS the hardware is cheap but the engineering efforts to get a working system are extensive. For load switching it is the other way around, expensive hardware and simpler engineering. To sell PSS equipment, it is in the interest of the manufacturers to underestimate the engineering efforts. Also, once the equipment is sold, the tuning of the PSS is the responsibility of the buyer, not the seller. Then academia comes in. They see the potential to interesting theoretical problems and to tell the PSS buyers how to do the tuning. This might explain why PSSs have been

around for 25 years but the power utilities still have problems to tune them. This has inspired us to try an alternative approach with load switching.

Figure 4. The hydro power station Hemsjö Övre.

5.2 Experiments

The purpose of the tests was to verify if load switching could be used to damp power oscillations. For this purpose, the grid configuration was changed so the hydro power station fed its power through a weak distribution system. A test program and an operation order for the network switching had been prepared and approved. Figure 4 shows the hydro power station at Hemsjö Övre.

The generator dynamics and inertia had been determined prior to the main tests. The load switching control and signal transmissions had been tested. Several practical arrangements had been made with the owner of the hydro power station and the local control center. Computer simulations had been done with Eurostag [5]. Tests had been made at small generators (1 kVA) in a laboratory at Lund Institute of Technology. We also had two constraints. The first was that our field test should not disturb the already low water flow in the river. The second constraint was that salmon were moving up the river for reproduction, and we were not allowed to disturb them. Eight persons participated in the test: two Ph.D. students; one relay engineer; one generator operator; one power station engineer; one engineer at the local control center; two technicians for switching in the distribution system.

Test Setup

Figure 5 shows the grid status during the tests.

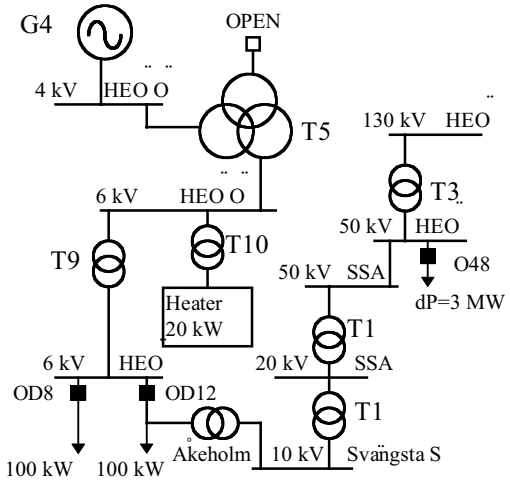

Figure 5. The grid status during the tests.

The two 100 kW loads in Figure 5 are countryside residential load. Figure 6 shows the test setup.

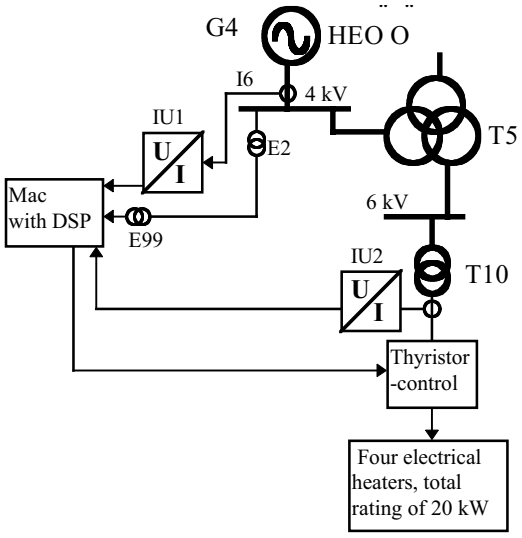

Figure 6. Test setup.

The components in Figure 6 are as follows:

- I6 is a permanent current transformer with ratio 150/5 A.
- IU1 is a temporarily installed clip-on current transformer type LEM, HEME PR30. The transducer gives 100 mV per ampere and the frequency range is from DC to 100 kHz. The maximal current is 20 A.
- E2 is a permanent voltage transformer with ratio 3850/110 V.
- E99 is a temporarily installed voltage transformer with ratio 220/7.67 V.

- IU2 is a temporarily installed clip-on current transformer type Kyoritsu, KEW 2004. The transducer gives 10 mV per ampere and the frequency range is from DC to 1 kHz. The maximal current is 200 A.

The three input signals were also recorded with a measurement computer of type Daqbook 200.

Digital Signal Processing and Control Algorithm

The block diagram in Figure 7 shows an overview of the calculation performed by the signal processor. The inputs are the generator current and voltage from phase *r*, and the load current in phase *r*. Appendix F contains a print-out of the Matlab code that was used to recreate signals from the raw data (U_gen_r, I_gen_t, I_load_r in Figure 7).

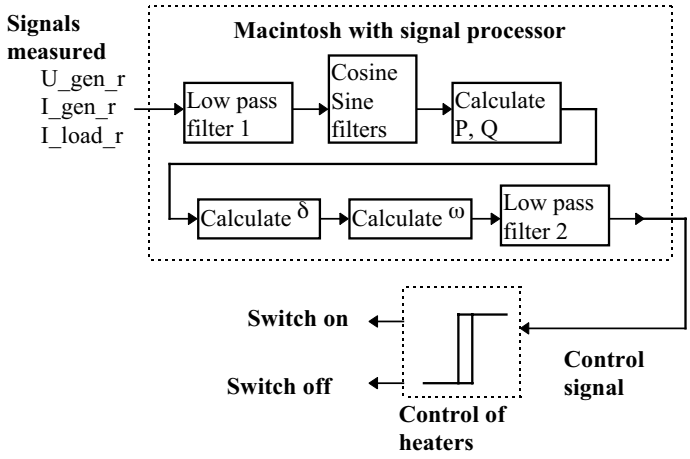

Figure 7. Overview of the signal processing. The angle δ is the angle between the generator's q-axis and the infinite bus.

The blocks in Figure 7 are as follows.

Low pass filter 1

Each input signal was pre-filtered in a FIR low pass filter. The filter used had a Hamming window with a length of 20 samples and the crossover frequency was 100 Hz. Figure 8 shows the filter frequency response.

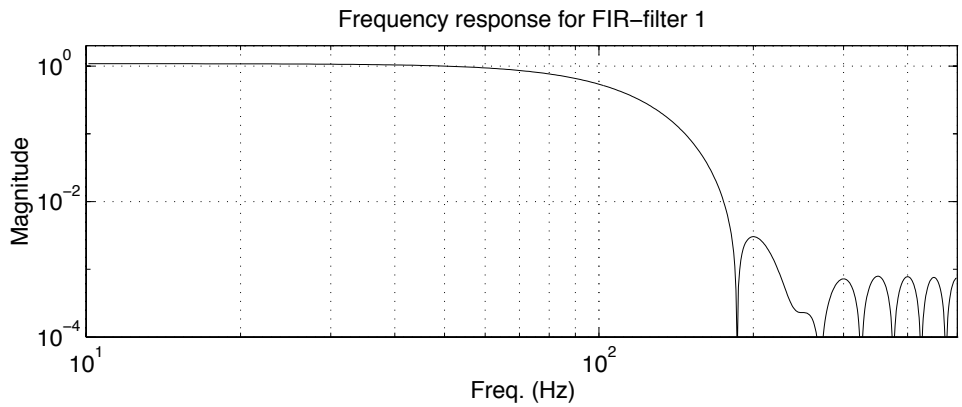

Figure 8. Frequency response for low pass filter 1.

Cosine and Sine filters

The purpose of the next operation is to get two orthogonal components that can be interpreted as a complex signal. Each input signal enters two FIR filters based on sine and cosine impulse response. The filter outputs have a phase difference of 90 degrees. At the system frequency (50 Hz) the filter gains are identical. For off nominal frequencies, the filter gains differ slightly. Figure 9 shows the gains and phase shifts for the two filters.

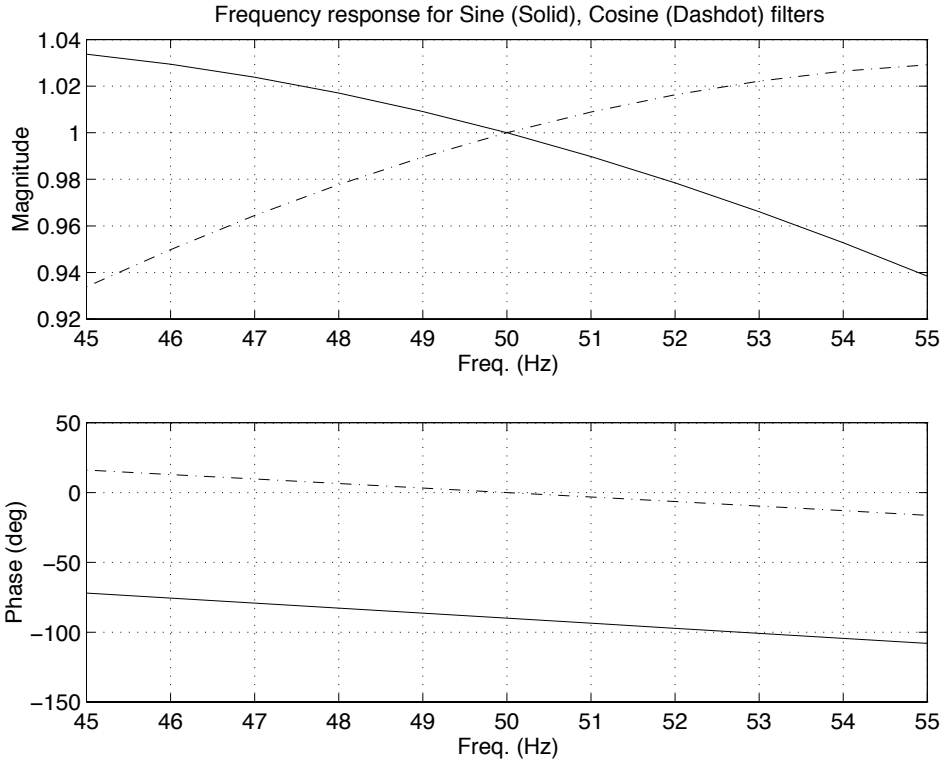

Figure 9. Frequency response for cosine and sine FIR filters.

The outputs are interpreted as real and imaginary parts of a complex signal. This method can also be used for frequency estimation, see Chapter 3 and reference [3.15]. The output from the Cosine, Sine block in Figure 7 are the three complex signals

$$\bar{I}_{gen} = I_{gen\,\mathrm{Re}} + j\, I_{gen\,\mathrm{Im}} \tag{1}$$

$$\overline{U}_{gen} = U_{gen\,\mathrm{Re}} + j\, U_{gen\,\mathrm{Im}} \tag{2}$$

$$\bar{I}_{load} = I_{load\,\mathrm{Re}} + j\, I_{load\,\mathrm{Im}} \tag{3}$$

where the subscripts *gen* and *load* have been used for generator and load.

Calculation of active and reactive power

The complex quantities from (1)-(3) are used to calculate the active and reactive power from the generator and load. The calculations for the generator are

$$P_{gen} = k \cdot \mathrm{Re}\left[\overline{U}_{gen} \cdot \overline{I}^{*}_{gen}\right] = k \cdot (U_{gen_{\mathrm{Re}}} \cdot I_{gen_{\mathrm{Re}}} + U_{gen_{\mathrm{Im}}} \cdot I_{gen_{\mathrm{Im}}}) \quad (4)$$

$$Q_{gen} = k \cdot \mathrm{Im}\left[\overline{U}_{gen} \cdot \overline{I}^{*}_{gen}\right] = k \cdot (-U_{gen_{\mathrm{Re}}} \cdot I_{gen_{\mathrm{Im}}} + U_{gen_{\mathrm{Im}}} \cdot I_{gen_{\mathrm{Re}}}) \quad (5)$$

where k is a calibration factor and * stands for complex conjugate. The power to the load is calculated in the same way. The power to the external grid—with subscript *grid*—is the difference between the generator output and the power to the load.

Calculation of the load angle δ

The generator load angle δ is the angle between the generator q-axis and a reference. We used the external 20 kV grid as our reference that was assumed to be infinitely strong compared to the generator. Resistance was neglected and the angle δ was calculated from the following steps:

$$\delta - \theta \leftarrow \arctan\left(\frac{\hat{x}_1 P_{gen}}{3\left|\overline{U}_{gen}\right|^2 + \hat{x}_1 Q_{gen}}\right) \quad (6)$$

$$-\theta \leftarrow \arctan\left(\frac{\hat{x}_3 P_{grid}}{3\left|\overline{U}_{gen}\right|^2 + \hat{x}_3 Q_{grid}}\right) \quad (7)$$

$$\delta \leftarrow (\delta - \theta) - (-\theta) \quad (8)$$

where

θ is the angle between the load bus and the reference;

$\hat{x}_1$ is the reactance between the load bus and the internal generator voltage;

$\hat{x}_3$ is the reactance between the load bus and the external grid.

Calculation of ω—change in load angle

The notation ω is used for change in load angle, that is

$$\omega = \frac{d}{dt}\delta(t). \quad (9)$$

The derivative is approximated by using two discrete samples of δ. The change in load angle is calculated as

$$\omega_k = \frac{(\delta_k - \delta_{k-1})}{h} \quad (10)$$

where h is the sampling interval, typically 1 ms.

Low pass filter 2

The difference approximation of ω tends to magnify noise. Before the signal is used as a control signal, it is low pass filtered in another FIR

filter. The filter used has a Hamming window with a length of 40 samples and the crossover frequency was 100 Hz. Figure 10 shows the filter frequency response.

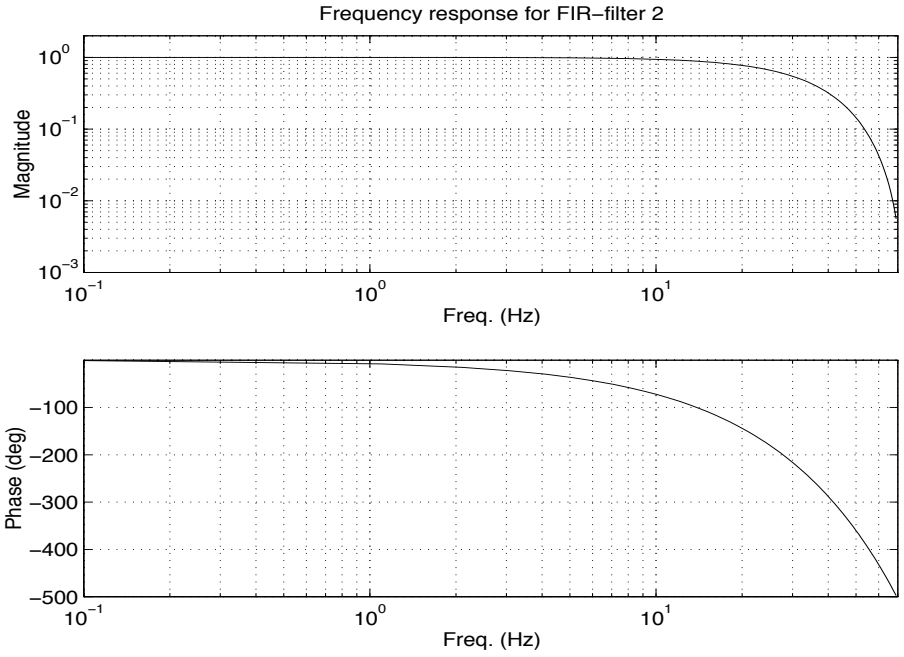

Figure 10. Frequency response for low pass filter 2.

The output signal from the Macintosh enters the thyristor unit that is described below.

Computer Equipment

Figure 11 shows the computer equipment used.

A Macintosh—Mac for short—boosted by a plug-in-card with a digital signal processor (DSP), Texas Instrument, TMS320C30, was used to calculate the control signal to the thyristor unit. The signal processor was programmed in C and the graphical user interface was made in LabView. Some of the quantities calculated were stored on the computer hard disk.

A portable PC with a measurement unit was used to store the raw signals that entered and left the Macintosh. The measurements unit was a Daqbook 200 with 16 inputs using a 16 bit AD converter. The sampling frequency was 2.0 kHz. The Daqbook was connected to the PC's parallel port. Four inputs were used for voltage measurement. The inputs had industrial "5B-modules" for signal conditioning and galvanic isolation.

Figure 11. Measurement equipment used at the field tests.

Thyristor Control

A specially designed thyristor unit was used to switch the heaters. The input to the unit was a voltage 0-5 volt, generated by the Mac. The unit had four individual steps, where the on and off levels can be individually set. Each step had a three-phase switch with a rating of 35 A at 380 V. Thus, the maximal rating for the thyristor unit was $4 \cdot \sqrt{3} \cdot 35 \cdot 380 = 90\,\text{kW}$. At the test, the switch-on level was 1.0 V and the switch-off level was 0.9 V.

Electrical Heaters

Figure 12 shows the four electrical heaters that were used. The rated power per heater was 15 kW at 380 V. The only available auxiliary power at the hydro station was 220 V, causing a power reduction to 5 kW per heater. Therefore, at the test we had a total of 20 kW available for control. The mechanical relays in the heaters were blocked in the on-state, so all switching was done from the thyristor control unit.

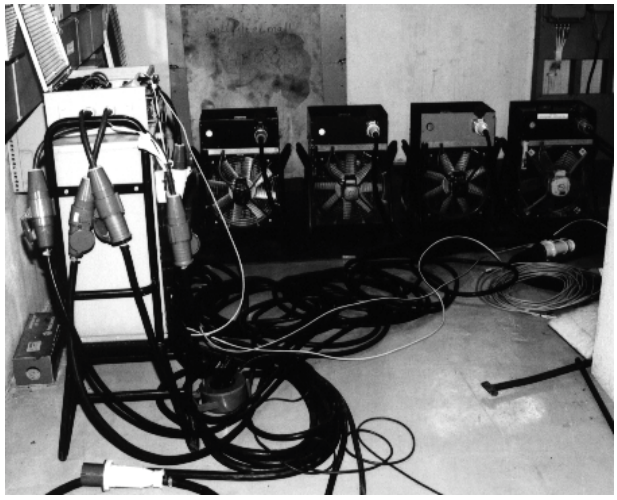

Figure 12. Thyristor control and electrical heaters.

Generators

The generators at Hemsjö Övre are not equipped with automatic voltage regulators (AVR). Each generator is magnetized from a rotating exciter that is manually controlled. Figure 13 shows the four generators and exciters.

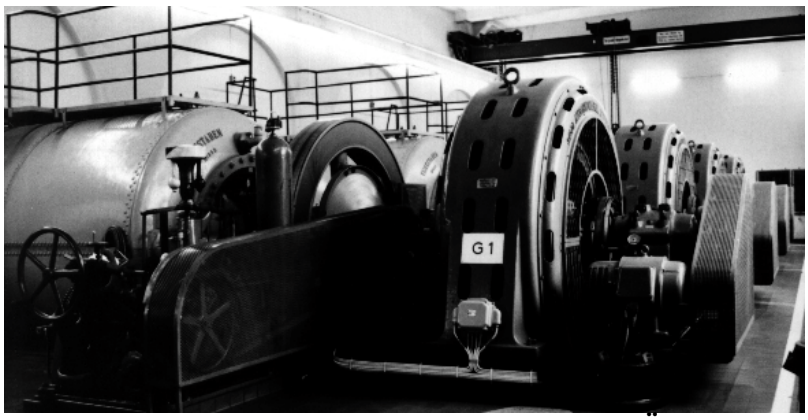

Figure 13. The generators at Hemsjö Övre.

Figure 14 shows the flyball governor that controls the turbine.

Figure 14. Turbine governor at Hemsjö Övre.

5.3 Results

A brief summary of the major test results is presented here. The complete measurement series are found in [3].

First Synchronization

When the generator was synchronized to the weak external grid, spontaneous power oscillations occurred. Since the purpose was to get a system with poor damping, the power oscillation was partly a success. In that sense we had made an almost too successful planning. Figure 15 shows that the generator was unstable since the oscillation amplitude is increasing. Reference [1] reports that there is a risk that a lightly loaded hydro power station connected to a weak grid can be unstable. The risk is pronounced if the generator lacks damper windings and if the connection to the grid has a high R/X ratio. These were exactly the conditions we experienced. A similar case has been reported in reference [2]. After around 60 seconds the amplitude was so large that the generator was manually disconnected from the grid.

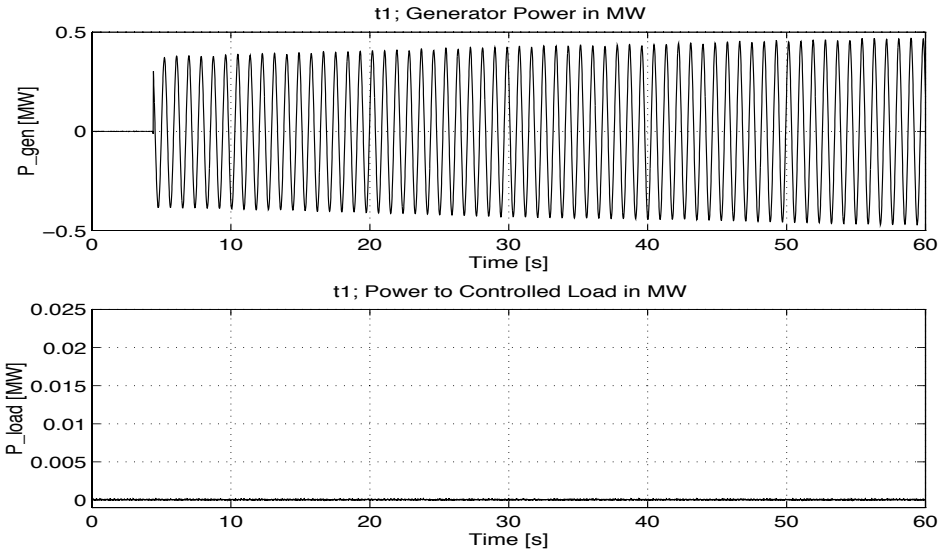

Figure 15. Power oscillations after first synchronization.

Synchronization with Additional Damping by Load Switching

We decided to make a new synchronization. The original plan was to successively test the control equipment. The experiment time table was extremely tight. The first synchronization had shown that without any control the system was unstable. To continue with the tests, the system had to be stabilized. The option we chose was to directly test the controlled load switching. The switching level in Figure 7 was set to 1 rad/s. Figure 16 shows that the controlled load switching worked perfectly at the initial test. This is believed to be unique.

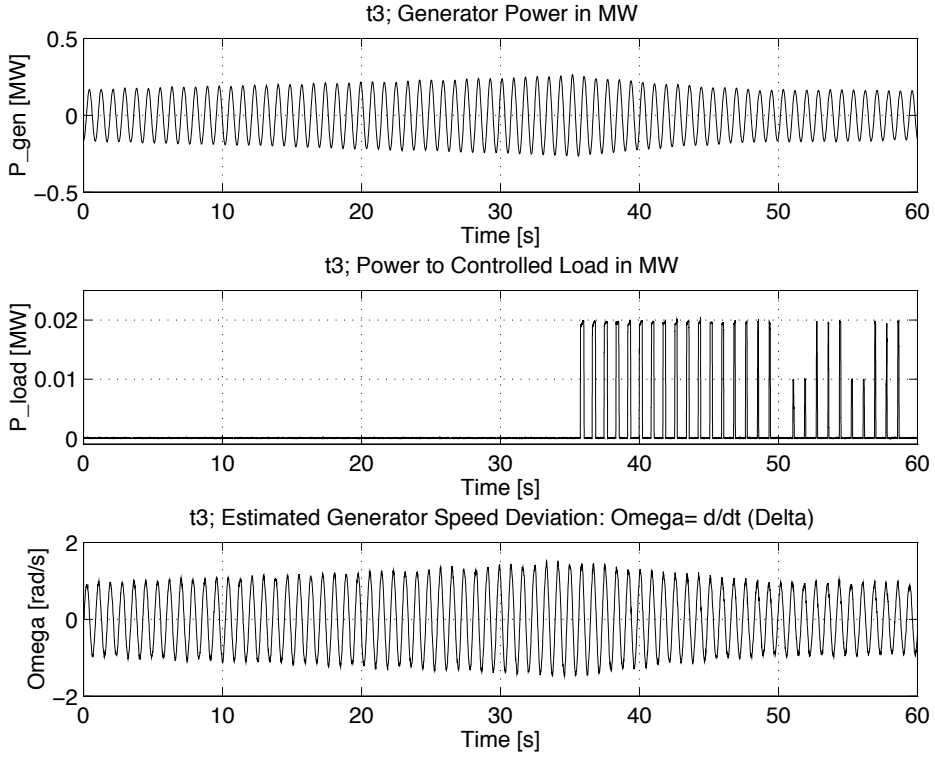

Figure 16. Second synchronization, the load switching is active for t > 35 s.

Figure 16 shows that the controlled load switching damps the power oscillation. The oscillation is stabilized so the switching level just reaches 1.0 rad/s.

Resonance

One part of the test program was to determine the resonance frequency. Figure 17 shows that the switching frequency 1.20 Hz is a resonance frequency. The generator operation point was 400 kW. The amplitude in power oscillation was still increasing, and had not reached the steady state value, when the switching was stopped. Please note that the rating of the load switched was only 20 kW and it caused the generator power to oscillate from nearly 200 to 600 kW.

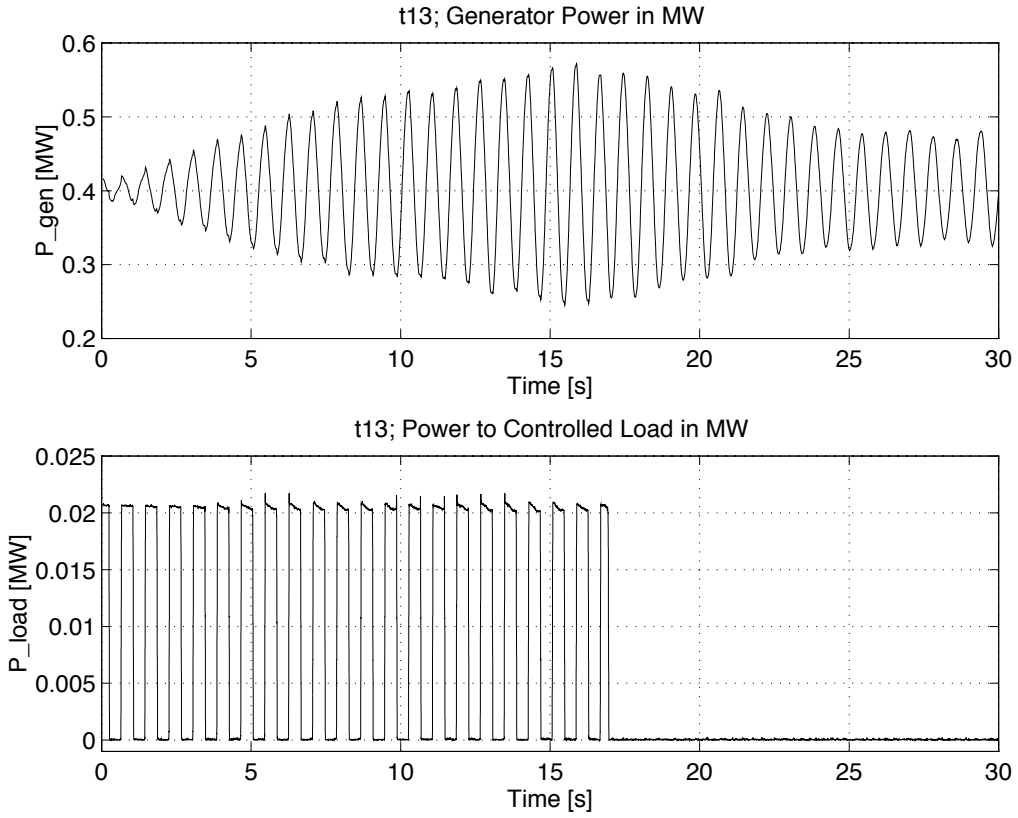

Figure 17. Power oscillations from load switching with the frequency 1.20 Hz.

Damping of Power Oscillation

Another way to verify the damping effect of load switching is to change the sign in the controller. A change of sign in a well tuned regulator should induce power oscillations. During the first 10 seconds in Figure 18, the regulator sign was changed. The figure clearly shows that the load switching builds up a power oscillation with increasing amplitude. Two measurements were done to compare damping with and without load switching. Figure 18 shows the damping without load switching.

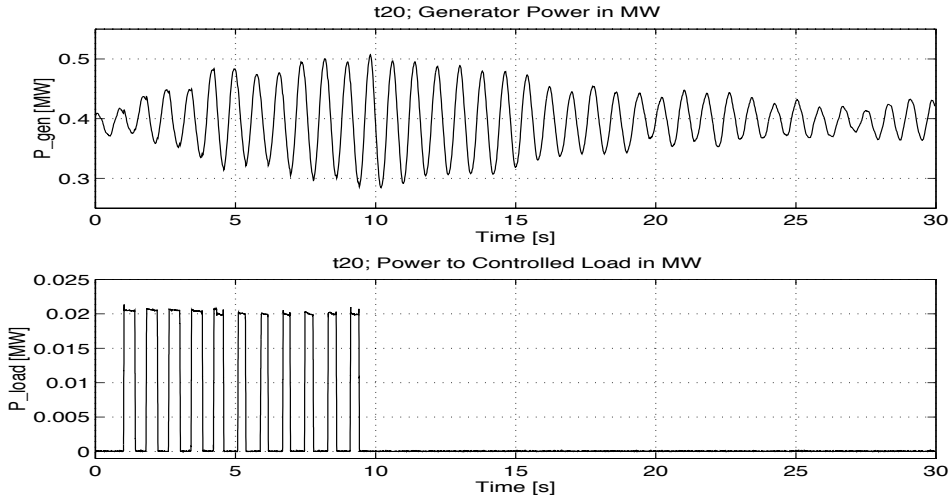

Figure 18. Excitation with load, damping without load switching.

Figure 19 shows the damping when load switching is used. It is evident that controlled load switching improves damping considerably.

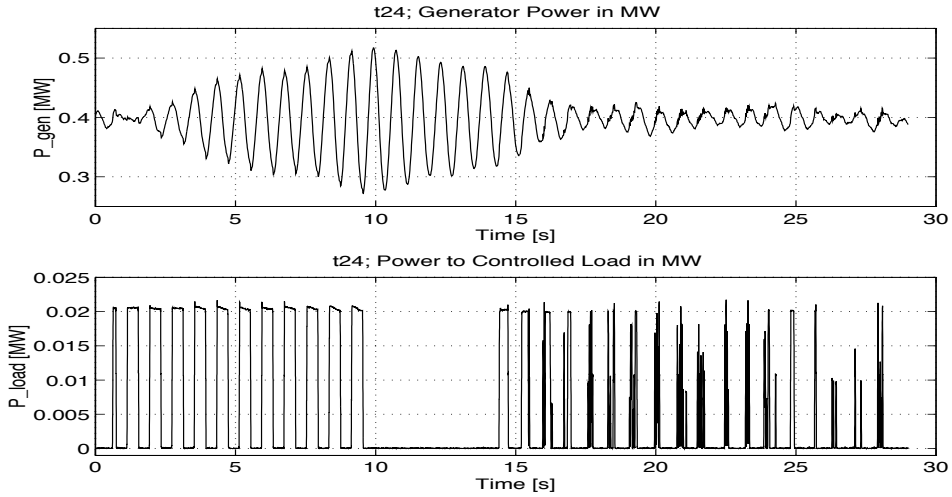

Figure 19. Excitation by load switching (1-9 s), thereafter no switching (9-14 s), then damping by controlled load switching (14-30 s).

Test Personnel

One key factor in field tests is skilled test personnel who know the local conditions. It seems favorable that participating personnel have overlapping skills. There is no obvious need for a cluster of theorists if nobody knows how to do the practical work. There is also a safety aspect. In a power station, a simple error such as opening a current circuit can have fatal consequences. Therefore several local technicians and operators from Hemsjo have been indispensable. Their names are listed in the acknowledgments.

5.4 References

[1] Kundur, P., *Power System Stability and Control*, McGraw-Hill, USA,1994.

[2] Crary, S. B., *Power System Stability*, Vol. II, John Wiley & Sons, Inc., USA, 1955.

[3] Akke, M., "Results from field tests at Hemsjo Ovre, September 24-25," (in Swedish), Sydkraft Report, PDK-9610-043, Malmo, Sweden, 1996.

[4] Samuelsson, O., “Structural Aspects of Controlling Active Power to Increase Power System Damping,” CODEN:LUTEDX/(TEIE-1014), Ph.D. thesis, Department of Industrial Electrical Engineering and Automation (IEA), Lund Institute of Technology, Lund, Sweden, to appear in May 1997.

[5] EUROSTAG User's manual - Release 2.3, Tractebel-Electricita, de France, Paris, France, April 1995.

[6] Akke, M., “Power System Stabilizers in Multimachine Systems,” Tech. Lic.-thesis, CODEN:LUTFD2/TFRT-3201/1-103/(1989), Department of Automatic Control, Lund Institute of Technology, Lund, Sweden, February, 1989.

[7] Paserba, J. et al., “CIGRE Technical Brochure on Control of Power System Oscillations”, CIGRE Task Force 38.01.07, Final Report Submitted to SC38 for Review, July, 1996.

[8] Heniche, A., Bourlès H. and Houry, M. P., “A Desensitized Controller for Voltage Regulation of Power Systems,” *IEEE Transaction on Power Systems*, Vol. 10, No. 3, August 1995, pp. 1461-1466.

[9] Lysfjord, T., Keränen, T., Messing, L., Østrup, T. and Ingemars, B., “Methods for tuning of PSS in Nordel,” (in Swedish), The Dynamic Group, Technical Report No. 2, April 30, 1984.

Appendix A

"Nonlinear Interaction of DC Cables and Magnetically Controlled Ship-Steering Autopilots," paper published in *IEEE Transaction on Control Systems Technology*, December 1995.

Not available in electronic format. Please see the reference.

Appendix B

"Frequency Estimation by Demodulation of Two Complex Signals," paper published in *IEEE Transaction on Power Delivery* (T-PWRD), January 1997.

Not available in electronic format. Please see the reference.

Appendix C

"Improved Estimates from the DEA by Median Post-Filtering," paper accepted to *IEE Conference on Developments in Power System Protection*, March 1997.

Not available in electronic format. Please see the reference.

Appendix D

"Some Improvements in the Three-phase Differential Equation Algorithm for Fast Transmission Line Relaying," paper submitted to *IEEE Power Engineering Society*, submitted January 1997.

SOME IMPROVEMENTS IN THE THREE-PHASE DIFFERENTIAL EQUATION ALGORITHM FOR FAST TRANSMISSION LINE PROTECTION

Magnus Akke, Member, IEEE
System Operation, Sydkraft AB
S-205 09 Malmo, Sweden

James T. Thorp, Fellow, IEEE
Cornell University
Ithaca, NY 14853-5401 USA

Abstract: This paper presents some improvements of the differential equation algorithm for transmission line protection. The improvements are: fault classification; new filtering; new algorithm for three-phase faults. Simulation results indicate a nominal operation time of 5-7 ms for three-phase faults and slightly higher for other fault types.

Keywords: digital relay, distance relay, differential equation, transmission lines.

I. INTRODUCTION

A. Background

Digital protection is often used for protection of transmission lines. Some techniques feasible for digital implementation are: symmetrical component [10]; differential equation algorithm (DEA) [1-7]; travelling wave algorithm. Algorithms based on phasors of the fundamental component use a Fourier calculation that requires around one cycle. A faster alternative is the differential equation algorithm (DEA) that can work with non-sinusoidal quantities. The frequency characteristics of voltage and current transformers put an upper limit on the DEA-performance. Research has been motivated by the belief that the DEA could reduce the operation time for a transmission line relay to _ cycle, i.e., around 5 ms. The operation time should include fault detection, estimation of fault location, fault classification, and tripping decision.

A number of factors influence the selection of a relaying algorithm for a specific transmission line relay. Issues of reliability, safety and speed must be considered. The DEA is suitable for an application where transient stability is the fundamental consideration. A fast DEA-relay together with a fast breaker, can reduce the fault clearing time to be within the critical time, thus maintaining system stability. When single pole tripping is used, most often a three-phase short-circuit close to the relay is the critical case that determines the limit for transient stability. Hence, such a relay needs an algorithm that can operate quickly for a three-phase fault within the first protection zone. With stability as a consideration, a slightly longer operation time can be accepted for other fault types. A relay based on the DEA is especially suitable when operation speed is crucial.

B. Contributions in this paper

In the paper we combine the fault location estimator with a Boolean fault classification. This results in one integrated algorithm. The idea has been borrowed from [10]. The key points presented in this paper are:

- a fault classification scheme for DEA that incorporates the equations for the different fault types into a unified fault estimator;
- speed improvements for three-phase faults, by using two equations with orthogonal quantities;
- improved filtering of the DEA estimates;
- simulation results indicate that the nominal operation time for a three-phase fault is 5-7 ms.

The first section presents the equation used in the DEA. Next, the fault classification scheme is developed. Then the resulting fault location and tripping condition are given. Simulation result follows, and the paper ends with a discussion and conclusions.

II. THE DIFFERENTIAL EQUATION ALGORITHM

Here we develop the algorithm used. We separate three different fault types: phase-to-earth; three-phase and two-phase fault. The equation for two-phase fault is valid both for phase-to-phase and two-phase-to-earth fault.

A. Presumptions

The presumptions used to derive the algorithm are:

- the line is short in the sense that it does not need to be modelled by surge impedance and wave propagation;
- the voltage and current transformer are ideal in the frequency range of the algorithm, 50-300 Hz;
- load current is neglected;
- the fault resistance is small;
- the line is perfectly transposed;
- shunt capacitance is neglected.

B. Derivation of general equations

Here we briefly derive the DEA, see [1]. With a desire to include the zero sequence resistance omitted in [2], we follow the derivation in [5]. A suitable reference on calculating sequence impedance is [9]. The faulty transmission line is modelled as:

$$\begin{pmatrix} v_a \\ v_b \\ v_c \end{pmatrix} = k_r R \begin{pmatrix} i_a \\ i_b \\ i_c \end{pmatrix} + k_l L \frac{d}{dt} \begin{pmatrix} i_a \\ i_b \\ i_c \end{pmatrix} \qquad (1)$$

where v_a, v_b, v_c and i_a, i_b, i_c are phase quantities. The parameter k_l and k_r are the relative line length for the resistive and the inductive part. For a fault on the line, both should be bounded between 0 and 1, and, for ideal conditions, they should be equal. The matrices R and L are the resistance and inductance matrix for the full line. We assume perfectly transposition, thus

$$R = \begin{pmatrix} R_s & R_m & R_m \\ R_m & R_s & R_m \\ R_m & R_m & R_s \end{pmatrix} \text{ and } L = \begin{pmatrix} L_s & L_m & L_m \\ L_m & L_s & L_m \\ L_m & L_m & L_s \end{pmatrix} \quad (2)$$

where the subscript s and m are used for self and mutual parameters. The superscript 0 and $+$ are used for zero and positive sequence. The relation between the parameters [9] are,

$$\begin{aligned} L^+ &= L_s - L_m \\ R^+ &= R_s - R_m \\ L^0 &= L_s + 2L_m \\ R^0 &= R_s + 2R_m. \end{aligned} \quad (3)$$

From (3) it follows that

$$\begin{aligned} 3L_m &= L^0 - L^+ \\ 3R_m &= R^0 - R^+. \end{aligned} \quad (4)$$

With use of (4) we rewrite equation (1) as

$$\begin{pmatrix} v_a \\ v_b \\ v_c \end{pmatrix} = k_r R^+ \begin{pmatrix} i_a \\ i_b \\ i_c \end{pmatrix} + k_l L^+ \frac{d}{dt}\begin{pmatrix} i_a \\ i_b \\ i_c \end{pmatrix} + k_r (R^0 - R^+)\begin{pmatrix} i_0 \\ i_0 \\ i_0 \end{pmatrix} + k_l (L^0 - L^+)\frac{d}{dt}\begin{pmatrix} i_0 \\ i_0 \\ i_0 \end{pmatrix} \quad (5)$$

where the zero sequence current is:

$$i_0 = (i_a + i_b + i_c)/3. \quad (6)$$

Next we derive the equations for each specific fault type. For all cases we neglect the voltage drop over any resistance at the fault location.

C. Phase-to-earth fault

Assume a fault on phase a to earth at the relative distance k of the line length.

$$v_a = k_r[R^+ i_a + (R^0 - R^+)i_0] + k_l[L^+ \frac{di_a}{dt} + (L^0 - L^+)\frac{di_0}{dt}] \quad (7)$$

The expression is written on the general form

$$v = k_r i_r + k_l \frac{di_l}{dt} \quad (8)$$

with

$$\begin{aligned} v &= v_a \\ i_r &= R^+ i_a + (R^0 - R^+)i_0 \\ i_l &= L^+ i_a + (L^0 - L^+)i_0. \end{aligned} \quad (9)$$

D. Phase-to-phase or two-phase-to-earth fault

Consider a fault between phase a and phase b at the distance k. If the fault has earth connection $i_0 \neq 0$, without earth connection $i_0 = 0$. In both cases, the equation is

$$\begin{pmatrix} v_a \\ v_b \end{pmatrix} = k_r R^+ \begin{pmatrix} i_a \\ i_b \end{pmatrix} + k_l L^+ \frac{d}{dt}\begin{pmatrix} i_a \\ i_b \end{pmatrix} + k_r (R^0 - R^+)\begin{pmatrix} i_0 \\ i_0 \end{pmatrix} + k_l (L^0 - L^+)\frac{d}{dt}\begin{pmatrix} i_0 \\ i_0 \end{pmatrix}. \quad (10)$$

The second row is subtracted from the first and we get

$$(v_a - v_b) = k_r R^+ (i_a - i_b) + k_l L^+ \frac{d}{dt}(i_a - i_b). \quad (11)$$

We write on the general form (8)

$$v = k_r i_r + k_l \frac{di_l}{dt}$$

with

$$\begin{aligned} v &= v_a - v_b \\ i_r &= R^+ (i_a - i_b) \\ i_l &= L^+ (i_a - i_b). \end{aligned} \quad (12)$$

E. Three-phase fault

Assume a symmetrical three-phase fault at the distance k. Since the fault is symmetrical, $i_0 = 0$, and

$$\begin{pmatrix} v_a \\ v_b \\ v_c \end{pmatrix} = k_r R^+ \begin{pmatrix} i_a \\ i_b \\ i_c \end{pmatrix} + k_l L^+ \frac{d}{dt}\begin{pmatrix} i_a \\ i_b \\ i_c \end{pmatrix}. \quad (13)$$

By using the αβ-components defined by

$$\begin{pmatrix} v_\alpha \\ v_\beta \end{pmatrix} = M \begin{pmatrix} v_a \\ v_b \\ v_c \end{pmatrix} \text{ with } M = \sqrt{\frac{2}{3}} \begin{pmatrix} 1 & -\frac{1}{2} & -\frac{1}{2} \\ 0 & \frac{\sqrt{3}}{2} & -\frac{\sqrt{3}}{2} \end{pmatrix} \quad (14)$$

the three phase quantities are condensed into two new quantities that are orthogonal in the sense that the two rows of M are orthogonal. We then have

$$\begin{pmatrix} v_\alpha \\ v_\beta \end{pmatrix} = k_r R^+ \begin{pmatrix} i_\alpha \\ i_\beta \end{pmatrix} + k_l L^+ \frac{d}{dt}\begin{pmatrix} i_\alpha \\ i_\beta \end{pmatrix}. \quad (15)$$

In the literature, the complete transformation is often called the αβ0-transform and then also includes the zero sequence component.

F. Solution of the equations

For the fault types: phase-to-earth, phase-to-phase and two-phase-to-earth we have the same general equation (8). The two unknown parameters k_l and k_r are estimated by this equation and three consecutive samples, see [1], [2]. The estimates are

$$\hat{k}_{r_n} = \frac{(i_{l_n} - i_{l_{n-1}})(v_{n-1} + v_{n-2}) - (i_{l_{n-1}} - i_{l_{n-2}})(v_n + v_{n-1})}{(i_{r_{n-1}} + i_{r_{n-2}})(i_{l_n} - i_{l_{n-1}}) - (i_{r_n} + i_{r_{n-1}})(i_{l_{n-1}} - i_{l_{n-2}})} \quad (16a)$$

$$\hat{k}_{l_n} = \frac{h}{2} \frac{-(i_{r_n} + i_{r_{n-1}})(v_{n-1} + v_{n-2}) + (i_{r_{n-1}} + i_{r_{n-2}})(v_n + v_{n-1})}{(i_{r_{n-1}} + i_{r_{n-2}})(i_{l_n} - i_{l_{n-1}}) - (i_{r_n} + i_{r_{n-1}})(i_{l_{n-1}} - i_{l_{n-2}})} \quad (16b)$$

where n is the time index.

For the three-phase fault we have two equations that are based on orthogonal quantities. Only two samples are needed to estimate the parameters. Straight forward calculations using the Tustin approximation for derivatives [12], gives the discrete-time equation system

$$\begin{pmatrix} i_{\alpha_n} + i_{\alpha_{n-1}} & i_{\alpha_n} - i_{\alpha_{n-1}} \\ i_{\beta_n} + i_{\beta_{n-1}} & i_{\beta_n} - i_{\beta_{n-1}} \end{pmatrix} \begin{pmatrix} k_r R^+ \\ k_l L^+ \frac{2}{h} \end{pmatrix} = \begin{pmatrix} v_{\alpha_n} + v_{\alpha_{n-1}} \\ v_{\beta_n} + v_{\beta_{n-1}} \end{pmatrix}. \quad (17)$$

The equation system is solved and the estimates are

$$k_{r_n} = \frac{1}{R^+} \cdot \frac{(i_{\beta_n} - i_{\beta_{n-1}})(v_{\alpha_n} + v_{\alpha_{n-1}}) - (i_{\alpha_n} - i_{\alpha_{n-1}})(v_{\beta_n} + v_{\beta_{n-1}})}{(i_{\alpha_n} + i_{\alpha_{n-1}})(i_{\beta_n} - i_{\beta_{n-1}}) - (i_{\alpha_n} - i_{\alpha_{n-1}})(i_{\beta_n} + i_{\beta_{n-1}})} \quad (18a)$$

and

$$k_{l_n} = \frac{h}{2} \frac{1}{L^+} \frac{-(i_{\beta_n} + i_{\beta_{n-1}})(v_{\alpha_n} + v_{\alpha_{n-1}}) + (i_{\alpha_n} + i_{\alpha_{n-1}})(v_{\beta_n} + v_{\beta_{n-1}})}{(i_{\alpha_n} + i_{\alpha_{n-1}})(i_{\beta_n} - i_{\beta_{n-1}}) - (i_{\alpha_n} - i_{\alpha_{n-1}})(i_{\beta_n} + i_{\beta_{n-1}})} \quad (18b)$$

G. Filtering of the estimates

Direct use of the above algorithm does not give acceptable estimates. Additional filtering of the estimates is crucial and is needed to yield something that can be used in a relay. It has been shown in [8] that at isolated points the DEA can become singular, giving extremely poor estimates. We use two remedies to cure the problem. First, the numerator and denominator are filtered separately before the division. Secondly, after the division, the fault location is filtered in a 7th-order median filter. The advantage with the median filter is that it totally rejects extreme values.

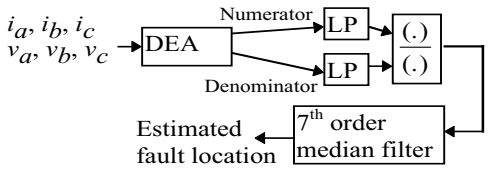

Fig. 1. Filtering of the DEA. LP stands for low pass filter.

The estimated fault location is the ratio between a numerator and a denominator, and it becomes singular if the denominator approaches zero. This effect is reduced by filtering the denominator before calculating the fault location. The numerator is also filtered in an identical filter, so the ratio is unchanged. Figures 2–4 illustrate the typical behaviour of the DEA, with and without filtering, for a three-phase short-circuit on a 170 km long 220 kV line.

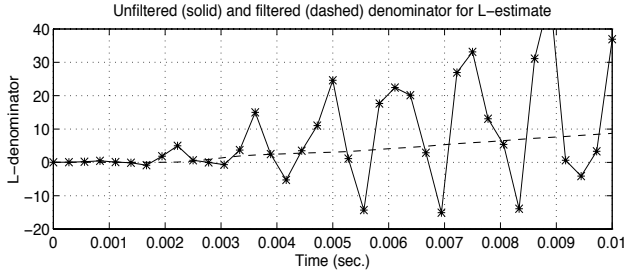

Fig. 2. Un-filtered (solid) and filtered (dashed) denominator for fault estimation based on inductance, i.e., k_l.

Fig. 2 shows that the un-filtered denominator oscillates around zero, taking both positive and negative values. With a bit of bad luck we could sample when the denominator is zero. A zero-division ruins the estimation. The dashed curve in Fig. 2, shows the filtered denominator. The oscillations are reduced and the denominator becomes smooth.

The un-filtered denominator is very close to zero just before 3 ms. The resulting fault location in Fig. 4 becomes a very poor estimate at this point. It can be shown that filtering before the ratio is calculated, results in a better fault estimate. Once the division is made, it is far more complicated to design a fast post-filter that reduces the effect of extremely poor values.

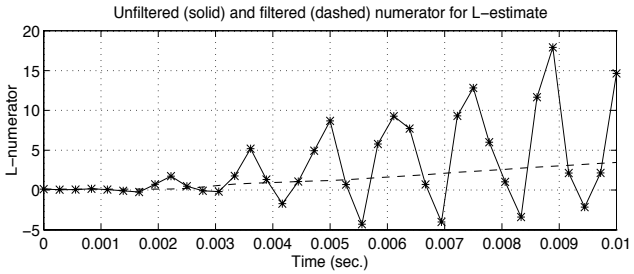

Fig. 3. Un-filtered (solid) and filtered (dashed) numerator for fault estimation based on inductance, i.e., k_l.

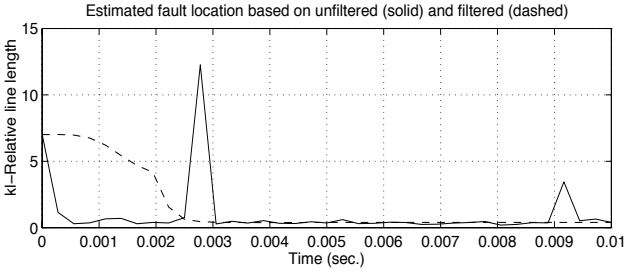

Fig. 4. Estimated fault location based on inductance, i.e., k_l.

III. Fault Classification

We use three Boolean indicators for fault classification. The objective is to make a classification that is fast, in particular for three-phase faults. Each indicator is treated in a separate section. Fig. 5 shows an overview of the fault classification used.

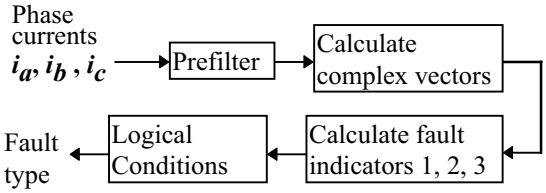

Fig. 5. Overview of the fault classification.

A. Pre-filters

The inputs to the fault classification are the three phase currents. Before sampled, each current has passed through an analogue anti-aliasing filter, consisting of a double RC-circuit, see [1]. The phase currents are then pre-filtered in a digital filter designed in Matlab [13]. The filter used is a 3:rd order Butterworth LP-filter, with cross-over frequency of 300 Hz, in cascade with an average filter. The average filter

restarts 2 ms after the fault detection and the filter length is increased until the full window length of 10 ms is reached.

B. Complex vectors

The phase currents are used to calculate complex vectors. The derivative of the phase current are used to form the imaginary part. The derivative is scaled, so that the amplitude of the real and imaginary parts are equal at the system frequency. For phase *a* the calculation is,

$$\bar{i}_a = i_a + j\frac{1}{\omega_0}\frac{d\,i_a}{dt} \tag{19}$$

The Tustin approximation is used in the digital implementation to approximate the derivative, see [12]. Thus we use the substitution

$$\frac{d}{dt} = \frac{2}{h}\frac{(1-q^{-1})}{(1+q^{-1})} \tag{20}$$

where q is the shift operator. Fig. 6 shows the calculation for phase *a*.

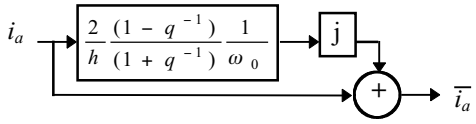

Fig. 6. Calculation of complex vectors.

The calculations for phase *b* and *c* are done in the same way.

C. Indicator 1

Indicator1 separates faults with zero sequence current from faults without zero sequence current. *Indicator1* is one for faults with zero sequence current and zero otherwise. The calculation is:

$$\begin{aligned} Value1 &= \frac{\left|\bar{i}_a + \bar{i}_b + \bar{i}_c\right|}{\text{median}(\left|\bar{i}_a\right|,\left|\bar{i}_b\right|,\left|\bar{i}_c\right|)} \\ Indicator1 &= \begin{cases} 1 \text{ if } Value1 > Limit1 \\ 0 \text{ otherwise} \end{cases} \end{aligned} \tag{21}$$

D. Indicator 2

Indicator2 is used for faults known to be without zero sequence current. It separates a three-phase fault from a phase-to-phase fault. *Indicator2* is one for a three-phase fault and is zero for a phase-to-phase fault. The calculation is:

$$\begin{aligned} Value2 &= \frac{\min\left(\left|\bar{i}_a + \bar{i}_b\right|,\left|\bar{i}_a + \bar{i}_c\right|,\left|\bar{i}_b + \bar{i}_c\right|\right)}{\text{median}\left(\left|\bar{i}_a + \bar{i}_b\right|,\left|\bar{i}_a + \bar{i}_c\right|,\left|\bar{i}_b + \bar{i}_c\right|\right)} \\ Indicator2 &= \begin{cases} 1 \text{ if } Value2 > Limit2 \\ 0 \text{ otherwise} \end{cases} \end{aligned} \tag{22}$$

E. Indicator 3

Indicator3 is used for faults known to have zero sequence current. It separates a phase-to-earth fault from a two-phase-to-earth fault. *Indicator3* is one for a phase-to-earth fault and zero for a two-phase-to-earth fault. The calculation is:

$$\begin{aligned} Value3 &= \frac{\text{median}\left(\left|\bar{i}_a\right|,\left|\bar{i}_b\right|,\left|\bar{i}_c\right|\right)}{\max\left(\left|\bar{i}_a\right|,\left|\bar{i}_b\right|,\left|\bar{i}_c\right|\right)} \\ Indicator3 &= \begin{cases} 1 \text{ if } Value3 < Limit3 \\ 0 \text{ otherwise} \end{cases} \end{aligned} \tag{23}$$

The three limits *Limit1*, *Limit2* and *Limit3* need to be set by the user. A suitable range can be determined by the quasi-stationary values for different fault types. It is important to consider different fault resistance, load current and even un-symmetrical load current. For example, *Value2* goes to zero for a phase-to-phase fault, and to one for a three-phase fault, that implies 0<*Limit2*<1. In the same way, it is straight forward to determine a reasonable range for the two other limits. Simulations can be used to check and refine the settings for a specific application. In the simulation example below we have used *Limit1*=0.05, *Limit2*=0.20 and *Limit3*=0.50.

F. Logical conditions for classification

The classification is made according to the following Boolean expressions.

$$B_{3\text{ph}} = \text{NOT(Indicator1) AND Indicator2}$$
$$B_{\text{ph-ph}} = \text{NOT(Indicator1) AND NOT(Indicator2)}$$
$$B_{\text{ph-ph-g}} = \text{Indicator1 AND NOT(Indicator3)}$$
$$B_{\text{ph-g}} = \text{Indicator1 AND Indicator3}$$

The notation B is used for a Boolean variable, that is either 0 or 1. The fault classification is also shown in Fig. 7.

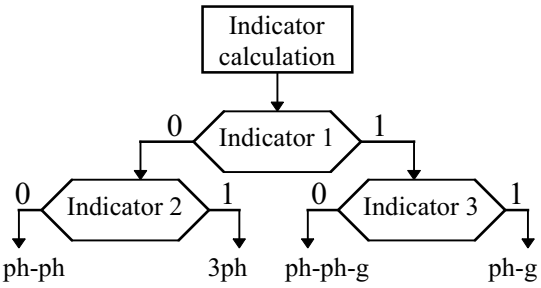

Fig. 7. Logical conditions for fault classification.

The time for fault classification is 2-3 ms for three-phase fault and slightly more for other fault types. The fault classification algorithm is calculated in parallel to the fault location schemes.

IV. Trip conditions

A. Resulting fault location

The fault location is estimated in parallel for all the four different fault types. The fault classification results in a logical variable that is one for the classified fault and zero for all other fault types. The resulting fault location is calculated as

$$\begin{aligned} k = {} & k_{\text{ph-ph}} \cdot B_{\text{ph-ph}} + k_{3\text{ph}} \cdot B_{3\text{ph}} \\ & + k_{\text{ph-ph-g}} \cdot B_{\text{ph-ph-g}} + k_{\text{ph-g}} \cdot B_{\text{ph-g}} \end{aligned} \tag{24}$$

where $k_{ph\text{-}ph}$ is the calculated fault location, and $B_{ph\text{-}ph}$ the

Boolean classification variable, either zero or one, for a phase-to-phase fault. The other notations are analogue.

B. Trip condition

The condition to generate the trip signal is as follow. First the counter limit (CL) is calculated as:

$$CL = T / h \tag{25}$$

where h is the sampling interval. The parameter T is a user determined parameter that can be interpreted as the shortest time delay for a fault at the beginning of the line. For each sample, the estimated fault location based on resistance and inductance are compared to a pre-set tripping zone. This tripping zone plays the same role as the R, X-zone for distance relays based on the 50 Hz component. If the calculated fault location is within the zone, a trip counter is increased. The increase is proportional to how close the fault is—one at the beginning of the line and zero at the boundary of the protected zone. The counter is decreased if the fault location is outside the zone. In our example we have used T=1 ms for a three-phase fault and 2 ms for other faults. A sampling interval of h=0.28 ms gives a counter limit of CL=3.57 for a three-phase fault.

V. Simulation results

The purpose of this section is to illustrate the DEA's performance under different conditions. Only the results for three-phase short-circuit are presented. The operation time for other fault types is slightly longer.

A. The model

The simulation and implementation of the DEA have been done in Matlab [13]. Fig. 8 shows the circuit used to model the faulted line and the connecting network.

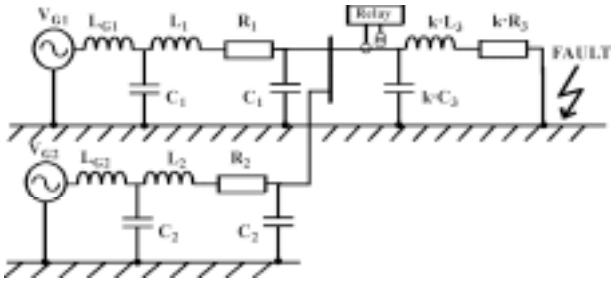

Fig. 8. The circuit used in the model.

Each line is modelled by a π-link. Typical sequence data for a Swedish 220 kV line are:

$$z^+ = 0.07 + j0.43 \ \Omega / \text{km}$$

$$z^0 = 0.52 + j1.45 \ \Omega / \text{km}$$

and the shunt capacitance

$$c^+ = 9.0 \cdot 10^{-9} \ \text{F} / \text{km}$$

$$c^0 = 7.0 \cdot 10^{-9} \ \text{F} / \text{km}.$$

The two connecting lines are 60 km and 80 km, respectively. The equivalent source reactance is $X_s = j\,26.5\ \Omega$. We neglect resistance and define the source impedance ratio (SIR),

$$SIR \approx \frac{X_s}{X_m} \tag{26}$$

where X_S is the equivalent source reactance and X_m is the reactance setting of the protected zone. The distance to fault (*DF*) is defined as

$$DF \approx \frac{X_l}{X_m} \tag{27}$$

where X_l is the reactance to the fault. Figures 9 and 10 show typical response for a three-phase short-circuit at 50% of the line length.

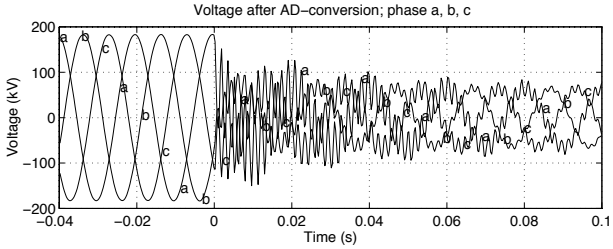

Fig. 9. Voltage after three-phase short-circuit.

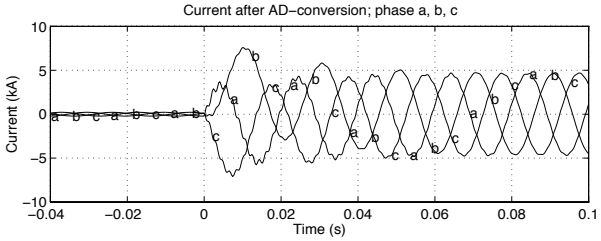

Fig. 10. Current after three-phase short-circuit.

B. Test cases

The operation time has been simulated for a three-phase fault at the location 10, 30, 50, 70, 80, 90, 95, 100 % of the protected zone. Two cases are presented here. In the first case, the line was not loaded and the protected line length was 30, 75, 150, 300 km, that corresponds to the source impedance ratios (*SIR*): 2.0; 0.8; 0.4; 0.2. In the second case, the line length was fixed to 30 km and four different load conditions were simulated, namely: light import (–46 MW, +5 Mvar); light export (+46 MW, –2 Mvar); high import (–136 MW, +14 Mvar); high export (+136 MW, –6 Mvar). Export is defined as power flowing from the relay location towards the remote end of the line.

The sampling was fast, 72 samples per period, that is 20/72=0.28 ms, or 5°. The operation time includes fault location, fault classification and tripping decision. The fault resistance was set to 1 ohm for all cases. The setting of the tripping zone was 80% of the line reactance in forward direction and 1000% of line resistance in both directions. For the tripping decision, the time delay T in (25) was 1 ms.

C. Results

Figures 11 and 12 summarise the results.

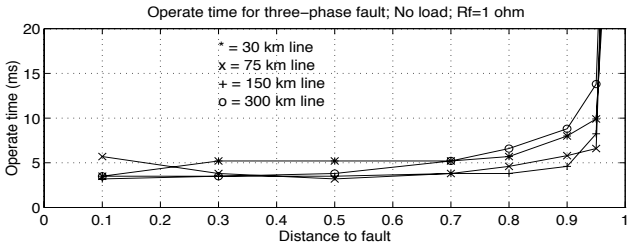

Fig. 11. Operate time for three-phase fault versus distance to fault for four different lengths of a 220 kV line.

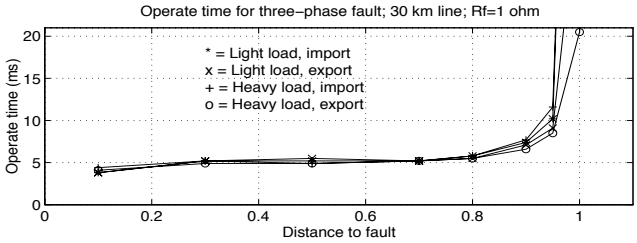

Fig. 12. Operate time for three-phase fault versus distance to fault for different operation conditions of a 30 km long 220 kV line.

VI. Discussion

Here we discuss some of the assumption and their influence on the results, what are the next steps and how far we can go in our conclusions.

The question of model validity should always be raised. In what frequency range is the model valid? The resistance and inductance are not independent of frequency. For example, both the zero sequence resistance and inductance are frequency dependent, see [9]. At higher frequencies the skin-effect becomes significant and increases the resistance of the lines. So it is important to understand that the model is best around the nominal system frequency and the accuracy is reduced as frequency increases.

The dynamics of voltage and current transformers have not been considered. Reference [14] presents suitable models and there is also on-going work within IEEE [15]. The dynamics of capacitive coupled voltage transformer (CCVT) are important for the relay algorithm as such and also for a directional relay. Remote end in-feed is not considered in the model. We should expect the same type of problem as for a conventional distance relay that estimates R and X. A better simulation model is needed, one possibility is to use EMTDC. Before doing any field test, the proposed DEA needs to be implemented and tested on a flexible development platform such as presented in [11].

Shunt capacitance is not considered in the DEA, but is used in the simulation model. The error due to this can be estimated from the charging current to the shunt capacitance. For a 300 km long 220 kV line, the charging current is around 100 A. In our example, a three-phase short-circuit at the remote end of the line gives a fault current of 817 A. In this case, it is obvious that the shunt capacitance will effect the algorithm's performance.

Start-criteria and directional relays are two topics that have deliberately been left out of the paper. The start-criteria needs to be very fast to detect a possible fault on the line and it should restart some of the filters used in the DEA. The task of the directional relay is to determine if the fault is in backward or forward direction. This feature is beneficial for faults close to the relay location. For these faults the estimated fault location k_l and k_r are very close to zero. Therefore the signs of k_l and k_r are an uncertain criteria to determine if the fault is on the line or not. In this situation the directional relay is especially useful. The directional relay determines if the trip counter should be increased or decreased, that is, the sign of the counter change. The fault location estimate should be used to determine the magnitude—not the sign—of the counter change.

VII. Conclusions

DEA is a promising method for transmission line protection where short clearing time is needed for three-phase faults. The paper has suggested the following improvements in the DEA:

- use of two equations based on orthogonal quantities to get fast three-phase fault location;
- a fault classification scheme that incorporates the equations for different fault types into a unified fault estimator;
- new filtering of the fault location estimates.

The simulation result implies that the operation time for source impedance ratios 0.2<SIR<2, is around 5-7 ms if the distance to fault is less than 80%. We hope to get the opportunity to do more simulations, prototype development and field tests, so that more far-going conclusions can be made.

VIII. Acknowledgement

Part of this work has been supported by a research grant from Sydkraft.

IX. References

[1] Phadke, A. G. and Thorp, J. S., *Computer Relaying for Power Systems,* Research Studies Press Ltd., Taunton, Somerset, England, 1994.

[2] Johns, A. T. and Salman, S. K., *Digital Protection for Power Systems,* Peter Peregrinus Ltd. on behalf of IEE, London, England, 1995.

[3] Breingan, W. D., Chen M. M. and Gallen T. F., "The Laboratory Investigation of a Digital System for the Protection of Transmission Lines," *IEEE Trans. on Power Apparatus and Systems*, Vol. PAS-98, No. 2, March/April, 1979, pp. 350-368.

[4] Jeyasuray, B. and Smolinski, W. J., "Identification of a Best Algorithm for Digital Distance Protection of Transmission Lines," *IEEE Trans. on Power Apparatus and Systems*, Vol. PAS-103, 1983, pp. 3358-3369.

[5] Ranjbar, A. M. and Cory, B. J., "An Improved Method for the Digital Protection of High Voltage Transmission Lines," *IEEE Trans. on Power Apparatus and Systems*, Vol. PAS-94, 1975, pp. 544-550.

[6] Smolinski, W. J., "An Algorithm for Digital Impedance Calculation Using a Single PI Section Transmission Line Model," *IEEE Trans. on Power Apparatus and Systems*, Vol. PAS-98, 1979, pp. 1546-1551.

[7] Ohura, Y. et al, "Digital Distance Relay with Improved Characteristics Against Distorted Transient Waveforms," *IEEE Trans. on Power Delivery*, Vol. 4, No. 4, 1989, pp. 2025-2031.

[8] Akke, M. and Thorp, J.S., "Improved Estimates from the Differential Equation Algorithm by Median Post-Filtering," accepted to *IEE Conference on Developments in Power Systems Protection*, The University of Nottingham, UK, 25-27 March, 1997.

[9] Anderson, P., *Analysis of Faulted Power Systems,* IEEE Press, Piscataway, NJ, USA, 1995.

[10] Phadke, A. G., Ibrahim, M & Hlibka, T.: "Fundamental Basis for Distance Relaying with Symmetrical Components", *IEEE Transaction on Power Apparatus and Systems*, Vol. PAS-96, No. 2, March/April, 1977, pp. 635-646.

[11] Sachdev, M. S. and Sidhu, T. S., "A Laboratory for Research and Teaching of Microprocessor-based Power Systems Protection", *IEEE Trans. on Power Systems*, Vol. 11, No. 2, May, 1996, pp. 613-619.

[12] Åstrom, K. J. and Wittenmark, B., *Computer Controlled Systems,* Prentice-Hall, Englewood Cliffs, USA, 1984.

[13] *Matlab-Reference Guide*, The MathWorks, Inc., Natick, Mass.

[14] Lucas, J. R. et al, "Improved Simulation Models for Current and Voltage Transformers in Relay Studies", *IEEE Trans. on Power Delivery*, Vol. 7, No. 1, January, 1992, pp. 152-159.

[15] McLaren, P. et al, "Mathematical Models for Current, Voltage and Coupling Capacitor Voltage Transformers", *Draft 2 to Working Group F10 of the Relay Input Sources Subcommittee*, Power System Relaying Committee, December 5, 1996.

X. BIOGRAPHIES

Magnus Akke (M'92) was born in Lund, Sweden 1961. He received his M.E.E degree and the Licentiate degree in Automatic Control, both from Lund Institute of Technology, Sweden, in 1986 and 1989, respectively. He also has a Bachelors degree in Business Administration from Lund University, Sweden. In 1990 he started at Sydkraft—a Swedish power utility—where his work tasks are power system analysis and relay protection. He has been a visiting scientist at University of Newcastle, Australia, and at Cornell University, USA. At present he is an industrial Ph.D. candidate, trying to apply control theory and signal processing to power systems.

James S. Thorp (SM'80, F'89) was born in Kansas City, Missouri on February 7, 1937. He received the B.E.E degree with distinction and the Ph.D. degree, both from Cornell University, Ithaca, New York in 1959 and 1962 respectively. In 1962 he joined the Cornell faculty, where he is currently Professor and Director of Electrical Engineering. In 1976 he was a faculty intern at the American Electric Power Service Corporation. He was an associate editor for IEEE Transactions on Circuits and Systems from 1985 to 1987. In 1988 he was an overseas fellow at Churchill College, Cambridge, England. In 1996 he was elected to the US National Academy of Engineering. He is a member of the IEEE Power System Relaying Committee, CIGRE, Eta Kappa Nu, Tau Beta Pi, and Sigma Xi. His research interests are protection and control of large-scale power systems including algorithms for digital protection, adaptive relaying, and real-time control of power systems using measurements obtained from microprocessor relays.

Appendix E

Proof of Equality Used in Statistical Calculations.

This appendix presents a proof of the relation

$$\frac{1}{\sqrt{2\pi}}\int_{-\infty}^{\infty}\frac{1}{x}\exp\left[-\frac{(x-m)^2}{2\sigma^2}\right]dx = \exp\left[-\frac{1}{2}(\frac{m}{\sigma})^2\right]\int_{0}^{m/\sigma}\exp(\frac{x^2}{2})\,dx$$

We start with

$$E\left[h(t)\right] = \int_{-\infty}^{\infty}\frac{1}{t}\frac{1}{\sigma\sqrt{2\pi}}\exp(-\frac{(t-m)^2}{2\sigma^2})dt = \int_{-\infty}^{\infty}h(t)\,f(t)\,dt \tag{1}$$

where

$$h(t) = \frac{1}{t} \tag{2}$$

$$f(t) = \frac{1}{\sigma\sqrt{2\pi}}\exp(-\frac{(t-m)^2}{2\sigma^2}) \tag{3}$$

We use Parseval's theorem—also known as Plancherel's theorem—that says that

$$\int_{-\infty}^{\infty}f(t)\overline{h}(t)\,dt = \frac{1}{2\pi}\int_{-\infty}^{\infty}F(\omega)\overline{H}(\omega)\,d\omega \tag{4}$$

where F and H are the Fourier transform of f and h respectively. The transforms are

$$F(\omega) = \exp(j\,m\omega - \frac{\omega^2\sigma^2}{2}) = \exp(-\frac{\omega^2\sigma^2}{2})\left(\cos(m\omega) + j\sin(m\omega)\right) \tag{5}$$

$$H(\omega) = \begin{cases} -j\pi; & \omega > 0 \\ j\pi; & \omega < 0 \end{cases} \tag{6}$$

We then have the problem

$$E = \frac{1}{2\pi}\int_{-\infty}^{\infty}F(\omega)\overline{H}(\omega)\,d\omega = \frac{1}{2\pi}\left[\int_{-\infty}^{0}F(\omega)(-j\pi)\,d\omega + \int_{0}^{\infty}F(\omega)(j\pi)\,d\omega\right]$$

$$= \frac{1}{2}\left[\int_{0}^{\infty}\exp(-\frac{\omega^2\sigma^2}{2})\sin(m\omega)\,d\omega - \int_{-\infty}^{0}\exp(-\frac{\omega^2\sigma^2}{2})\sin(m\omega)\,d\omega\right] \tag{7}$$

$$-\frac{j}{2}\left[\int_{0}^{\infty}\exp(-\frac{\omega^2\sigma^2}{2})\cos(m\omega)\,d\omega - \int_{-\infty}^{0}\exp(-\frac{\omega^2\sigma^2}{2})\cos(m\omega)\,d\omega\right]$$

Because of the of the odd and even symmetry of sinus and cosine we get

$$E = \int_{0}^{\infty}\exp(-\frac{\omega^2\sigma^2}{2})\sin(m\omega)\,d\omega \tag{8}$$

This integral is continuous for all ω and is therefore easier to calculate than (1). We write E as the imaginary part of the complex integral I

$$E = \mathrm{Im}(I)$$

where the integral is

$$I = \int_0^\infty \exp(-\frac{\omega^2\sigma^2}{2}) \exp(jm\omega)\, d\omega = \int_0^\infty \exp(-\frac{\omega^2\sigma^2}{2} + jm\omega)\, d\omega \tag{10}$$

to complete the squares we rewrite (10) as

$$I = \exp(-\frac{1}{2}\frac{m^2}{\sigma^2}) \int_0^\infty \exp(-\frac{\left[\omega\sigma - j\frac{m}{\sigma}\right]^2}{2}) d\omega \tag{11}$$

We make the variable substitution

$$\begin{aligned} y &= \omega\sigma - j\frac{m}{\sigma} \\ d\omega &= \frac{1}{\sigma} dy \end{aligned} \tag{12}$$

and change the integration limits accordingly

$$\begin{aligned} \omega = 0 &\Leftrightarrow y = -j\frac{m}{\sigma} \\ \omega = \infty &\Leftrightarrow y = \infty - j\frac{m}{\sigma} \end{aligned} \tag{13}$$

We then have the new integral in y

$$I = \exp(-\frac{1}{2}\frac{m^2}{\sigma^2}) \frac{1}{\sigma} \int_{-j\frac{m}{\sigma}}^{\infty - j\frac{m}{\sigma}} \exp(-\frac{y^2}{2})\, dy \tag{14}$$

We focus on the integral in y and call this for I_y, i.e.,

$$I_y = \int_{-j\frac{m}{\sigma}}^{\infty - j\frac{m}{\sigma}} \exp(-\frac{y^2}{2})\, dy \tag{15}$$

Now we use that

$$\oint_\gamma \exp(-\frac{y^2}{2}) dy = 0 \tag{16}$$

if the function has no singularities inside the closed contour γ.

We choose a rectangular contour γ that consists of four parts, $\gamma = \gamma_1 + \gamma_2 + \gamma_3 + \gamma_4$ where

$$\gamma_1 : y = 0 - j\beta \quad \text{with} \quad 0 < \beta < \frac{m}{\sigma}$$

$$\gamma_2 : y = \alpha - j\frac{m}{\sigma} \quad \text{with} \quad 0 < \alpha < \infty$$

$$\gamma_3 : y = \infty - j\beta \quad \text{with} \quad 0 < \beta < \frac{m}{\sigma}$$

$$\gamma_4 : y = \alpha \quad \text{with} \quad 0 < \alpha < \infty \tag{17}$$

The contour is illustrated in Figure 1.

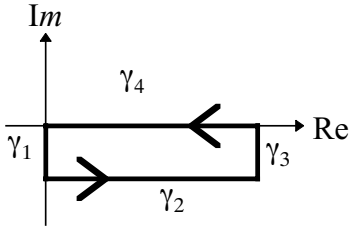

Figure 1. Contour for integration

We choose to integrate around the contour in anti-clockwise direction (if any reader knows the direction of a rectangular clock).

$$\int_{\gamma_1} \exp(-\frac{y^2}{2})dy = -j\int_0^{m/\sigma} \exp(\frac{y^2}{2})dy \tag{18}$$

$$\int_{\gamma_3} \exp(-\frac{y^2}{2})dy = 0 \tag{19}$$

$$\int_{\gamma_4} \exp(-\frac{y^2}{2})dy = \int_{\infty}^{0} \exp(-\frac{y^2}{2})dy = -\int_0^{\infty} \exp(-\frac{y^2}{2})dy = -\sqrt{\frac{\pi}{2}} \tag{20}$$

We find the integral we are interested in by

$$I_y = \int_{-j\frac{m}{\sigma}}^{\infty - j\frac{m}{\sigma}} \exp(-\frac{y^2}{2})\, dy = \int_{\gamma_4} \exp(-\frac{y^2}{2})dy =$$

$$= -\int_{\gamma_1+\gamma_2+\gamma_3} \exp(-\frac{y^2}{2})dy = -(-\sqrt{\frac{\pi}{2}} - j\int_0^{m/\sigma} \exp(\frac{y^2}{2})dy) \tag{21}$$

We put our results together and find that

$$I = \frac{1}{\sigma}\exp(-\frac{1}{2}\frac{m^2}{\sigma^2})\left[+\sqrt{\frac{\pi}{2}} + j\int_0^{m/\sigma} \exp(\frac{y^2}{2})dy\right] \tag{22}$$

and finally

$$E\left[h(t)\right] = I\mathrm{m}(I) = \frac{1}{\sigma}\exp\left[-\frac{1}{2}(\frac{m}{\sigma})^2\right]\int_0^{m/\sigma}\exp(\frac{y^2}{2})dy\,. \qquad (23)$$

We co*m*pare (1) with (23) an*d* fin*d* the relation

$$\frac{1}{\sqrt{2\pi}}\int_{-\infty}^{\infty}\frac{1}{\mathrm{x}}\exp\left[-\frac{(\mathrm{x}-m)^2}{2\sigma^2}\right]d\mathrm{x} = \exp\left[-\frac{1}{2}(\frac{m}{\sigma})^2\right]\int_0^{m/\sigma}\exp(\frac{\mathrm{x}^2}{2})\,d\mathrm{x}\,. \qquad (24)$$

Alternative proof

After the proof was written down, my colleague Bob showed me a shorter alternative that does not need an excursion into Fourier territory. We start to take the derivative with respect to y of the following expression

$$\frac{d}{dy}\int_{-\infty}^{\infty}\frac{1}{x}\exp(\frac{-x^2+2yx}{2\sigma^2})\,dx$$
$$=\frac{1}{\sigma^2}\int_{-\infty}^{\infty}\exp(\frac{-x^2+2yx}{2\sigma^2})\,dx=\frac{\sqrt{2\pi}}{\sigma}\exp(\frac{y^2}{2\sigma^2}) \tag{25}$$

Integration from 0 to m of the left hand side of (25) with respect to y gives

$$\int_0^m\left(\frac{d}{dy}\int_{-\infty}^{\infty}\frac{1}{\mathrm{x}}\exp(\frac{-\mathrm{x}^2+2y\,\mathrm{x}}{2\sigma^2})\,d\mathrm{x}\right)dy=\left[\int_{-\infty}^{\infty}\frac{1}{\mathrm{x}}\exp(\frac{-\mathrm{x}^2+2y\,\mathrm{x}}{2\sigma^2})d\mathrm{x}\right]_{y=0}^{y=m}=$$
$$\int_{-\infty}^{\infty}\frac{1}{\mathrm{x}}\exp(\frac{-\mathrm{x}^2+2m\,\mathrm{x}}{2\sigma^2})\,d\mathrm{x}-\int_{-\infty}^{\infty}\frac{1}{\mathrm{x}}\exp(-\frac{\mathrm{x}^2}{2\sigma^2})\,d\mathrm{x}= \tag{26}$$
$$\int_{-\infty}^{\infty}\frac{1}{\mathrm{x}}\exp(\frac{-\mathrm{x}^2+2m\,\mathrm{x}}{2\sigma^2})\,d\mathrm{x}$$

Identical integration of the right hand side of (25) and a variable substitution gives

$$\frac{\sqrt{2\pi}}{\sigma}\int_0^m\exp(\frac{y^2}{2\sigma^2})\,dy=\sqrt{2\pi}\int_0^{m/\sigma}\exp(\frac{\mathrm{x}^2}{2})\,d\mathrm{x} \tag{27}$$

We multiply (26) and (27) by $\frac{1}{\sqrt{2\pi}}\exp(-\frac{m^2}{2\sigma^2})$ and get the equality

$$\frac{1}{\sqrt{2\pi}}\int_{-\infty}^{\infty}\frac{1}{x}\exp(-\frac{(x-m)^2}{2\sigma^2})\,dx=\exp(-\frac{m^2}{2\sigma^2})\int_0^{m/\sigma}\exp(\frac{x^2}{2})\,dx \tag{28}$$

that is identical to (24).

Appendix F

Field Test in Hemsjö—Matlab Code to Recreate Signals From Raw Data

```
% Macro to process raw data from field tests at Hemsjö 24 sept, 1996.
clear all; close all;
x1hat=7; % (Ohm), generator reactance
x3hat=3; % (Ohm), external network reactance
fs=1000; % sampling frequency in Hz
f0=50; % Nominal frequency
N=fs/50;
No=input('Enter test no ===>');
eval(['load t' num2str(No)]);
%
% take out variables and calibrate
c1=5*(150/5)*10;
% voltage calibration in kV
c2=(1e-3)*(3850/110)*(132.5)/(4.62);
% load current at 4 kV level, ratio aux. power + ratio T5
c3=1000*(0.22/6)*(6.3/3.6);
%
% i1=generator current; u=generator voltage; i2=load current
eval(['i1=c1*' VarName '(:,1);']);
eval(['u=c2*' VarName '(:,2);']);
eval(['i2=c3*' VarName '(:,3);']);
%
NN=length(i1); h=1/fs;  t=[0:h:(NN-1)*h];
%
% FIR low pass filter
% adjust gain so magnitude is unity at 50 Hz
% Default window is Hamming
B=(1/0.919)*fir1(N,0.2); % Window=20; cross over =0.2*fn=100 Hz; fn=fs/2;
A=[1 zeros(1,N-1)];
%
i1=filter(B,A,i1);
u=filter(B,A,u);
i2=filter(B,A,i2);
%
% COS and SIN filter i1 and u
dphi=2*pi/N;  phi=[0:dphi:(N-1)*dphi];
B_COS=(sqrt(2)/N)*cos(phi);  B_SIN=(sqrt(2)/N)*sin(phi);
%
i1_re=filter(B_COS,A,i1);   i1_im=filter(B_SIN,A,i1);
%--
u_re=filter(B_COS,A,u);  u_im=filter(B_SIN,A,u);
%--
i2_re=filter(B_COS,A,i2);  i2_im=filter(B_SIN,A,i2);
%
i2_abs=sqrt(i2_re.*i2_re+i2_im.*i2_im);   % A at 4 kV
u_abs=sqrt(u_re.*u_re+u_im.*u_im); % kV
i1_abs=sqrt(i1_re.*i1_re+i1_im.*i1_im);   % A
%
i2_re=i2_abs.*(u_re./u_abs);
```

```
i2_im=i2_abs.*(u_im./u_abs);
%
% Change to p.u.
u_bas=3.850/sqrt(3);        u_pu=u_abs./u_bas;
i1_bas=880/(sqrt(3)*3.85); i1_pu=i1_abs./i1_bas;
%
% generator
p1=(1e-3)*3.0*(u_re.*i1_re+u_im.*i1_im);  % MW
q1=(1e-3)*3.0*(-u_re.*i1_im+u_im.*i1_re); % MVAr
% load
p2=(1e-3)*3.0*(u_re.*i2_re+u_im.*i2_im);  % MW
% q2 should be 0, since resistive load
q2=(1e-3)*3.0*(-u_re.*i2_im+u_im.*i2_re);  % MVAr
% external net
p3=p2-p1;   q3=q2-q1;
%
% Angles
phi=atan2(q1,p1);
delta_teta=atan2(x1hat*p1,3.0*u_abs.*u_abs+x1hat*q1);
minus_teta=atan2(x3hat*p3,3.0*u_abs.*u_abs+x3hat*q3);
delta=delta_teta-minus_teta;
%
% Estimation of omega= d/dt (delta)
omega=(1/h)*[0; diff(delta)];
%
% FIR low pass filter of omega
% adjust gain so magnitude is unity at 1 Hz
% Default window is Hamming
B_LP=fir1(2*N,0.06); % Window=40; cross over =0.06*fn=30 Hz
A_LP=[1 zeros(1,2*N-1)];
omega=filter(B_LP,A_LP,omega);
```